A Network-based approach for Quantifying the Resilience and Vulnerability of HIV-1 Native Glycan Shield

Srirupa Chakraborty[1,2,5], Zachary T. Berndsen[3,4,5], Nicolas W. Hengartner[1], Bette T. Korber[1], Andrew B. Ward[3,4,6], and S. Gnanakaran[1,6]

[1]Theoretical Biology & Biophysics, Los Alamos National Laboratory, Los Alamos, NM 87545, USA
[2]Center for Non-Linear Studies, Los Alamos National Laboratory, Los Alamos, NM 87545, USA
[3]Department of Integrative Structural and Computational Biology, The Scripps Research Institute, La Jolla, CA 92037, USA
[4]IAVI Neutralizing Antibody Center and Collaboration of AIDS Vaccine Discovery, The Scripps Research Institute, La Jolla, CA 92037, USA

[5]These authors contributed equally

[6]Lead Contacts: andrew@scripps.edu, gnana@lanl.gov

Summary

The dense arrangement of N-glycans masking antigenic surfaces on the HIV-1 envelope (Env) protein acts as a shield from the adaptive immune system. The molecular complexity of glycan modifications and their inherent dynamic heterogeneity on a protein surface make experimental studies of glycoprotein structures a challenge. Here we have integrated a high-throughput atomistic modeling with graph-theory based method to capture the native glycan shield topological network and identify concerted behavior of these glycans. This is the first time that a complete computational model of an HIV-1 Env trimeric SOSIP structure has been generated with a native glycosylation pattern including both oligomannose and complex glycans, thus obtaining results which are immunologically more relevant. Important global and local feature differences due to the native-like glycosylation pattern have been identified, that stem from the charged sialic acid tips, fucose rings at the base, and different branching patterns of the complex glycans. Analyses of network attributes have aided in detailed description of the shield in a biological context. We have also derived a measure to quantify the shielding effect based on the number of glycan heavy atoms encountered over the antigenic protein surface that can define regions of relative vulnerability and resilience on the shield, and can be harnessed for potential immunogen design.

Introduction

Protein glycosylation is an essential aspect of post-translational modification, with 50-70% of human proteins been estimated to be glycosylated to some degree[1]. These glycans play significant roles in numerous biological processes, such as cellular signaling, recognition and adhesion, protein folding, structural stability, and immune system interactions[2-4]. A detailed comprehension of the three-dimensional structure and dynamics of these glycan moieties is essential for a thorough understanding of the molecular basis of such functions. One of the most frequently occurring protein glycosylation type found in nature is where the glycan moieties are covalently attached to protein at asparagine (N) residues by an N-glycosidic bond. Investigation of protein databases suggest that ~70% of proteins carry one or more motifs required for potential N-glycosylation sites (PNGS, given by the sequon Asn-X-[Ser or Thr], where X is not proline)[5]. Such glycans usually have about 10-20 pyranose rings covalently connected in a tree-like structure to the asparagine residue of the sequon. An important function of N-glycosylated proteins is their role in viral and other pathogen-host relationships[6-9], making them a major focus for biomedical research efforts.

Envelope proteins from several high-risk viral pathogens, such as HIV (lentivirus)[10], Lassa (arenavirus)[11], Hepatitis C (flavivirus)[12], Epstein Barr (herpesvirus)[13], Ebola (filovirus)[14, 15], and Influenza[8] are heavily glycosylated, where the host protein production and glycosylation machineries are hijacked by these viruses. These surface-expressed viral proteins are important immunological targets for neutralizing antibodies that can block viral infection of cells, and form the primary focus of vaccine studies[16, 17]. However, the dynamic and dense glycan coating can effectively act as a shield for the underlying envelope protein, masking antigenic surfaces, barricading it from the adaptive immune system, and defending against immune surveillance[18-23].

A deeper molecular level understanding of the glycan shields in these pathogenic viruses may help inform vaccine design strategies that can overcome this protective barrier. However, glycoproteins as a class remain recalcitrant to structural studies. The extreme dynamic heterogeneity and conformational complexity stemming from large variance of possible constituent sugars, linkage, branching patterns, and rotamer flexibility, make the study of these

glycans immensely challenging[24, 25]. High internal flexibility within each glycosidic bond and the compositional heterogeneity of the glycans prevent proper crystallization of these glycoproteins, rendering traditional X-ray crystallography methods ineffectual[26]. The inherent flexibility within glycan chains also makes structural determination by Nuclear Magnetic Resonance (NMR) and cryo-Electron Microscopy (cryo-EM) techniques challenging and incomplete[26-29]. Considering the case of HIV-1 alone, currently there are more than 300 experimental structures of envelope glycoprotein in the Protein Databank[30]. However, at best, only a quarter of the total envelope glycan content has been structurally resolved. Most of these were coordinated by antibodies and stabilized away from the true dynamic picture of the native trimer, providing little information about the structural and dynamic details of the surface glycans.

Computational modeling and molecular dynamics (MD) simulations have been particularly useful as a complementary approach towards the characterization of such systems[31-34], and have been harnessed to study the conformational dynamics of the HIV Env glycan shield[18, 35-37]. However, the main drawback affecting the quality of MD simulations is the robustness of conformational sampling. Due to the intrinsically dynamic nature of glycans, to effectively sample a biologically relevant energy landscape of the glycoprotein long and often multiple trajectories need to be run, preferably with enhanced sampling techniques[36]. Such simulations for a system as large as the HIV-1, Ebola and other viral glycoproteins requires extensive computational power and time. We have previously established a high throughput pipeline to robustly build atomistic models of glycans, sample the glycan conformational space, construct the glycan network topology, and extract a molecular level description of the viral glycan shield[38]. In that study, we had also extensively validated the modeled ensembles against experimental cryo-EM data. This method drastically improves conventional sampling time, and yet retains the necessary accuracy to be physiologically relevant.

Here, we have applied our network modeling methodology on the HIV-1 Envelope Glycoprotein (Env) with a native glycosylation pattern. The Env is a heterodimeric trimer composed of proteins gp120 and gp41, and is responsible for the molecular recognition of the host receptor and fusion into host target cells. A number of obstacles hinder traditional vaccine design methods in case of HIV-1 – namely its remarkable sequence diversity, conformational plasticity, dramatic shifts in position and number of PNGS[39], and extremely dense glycosylation patterns

making up to approximately half the mass of the entire Env molecule[40]. As a result, there has been only limited success in eliciting broadly neutralizing antibodies (bNAbs) to Env vaccine immunogens[41-43]. These sugar moieties are highly dynamic[29], and have a median of 93 N-linked glycans present per HIV-1 trimer[18]. Structures of bNAbs in complex with Env indicate that these antibodies need to extend through the glycan shield in order to engage with the epitopes at the protein surface[44-47]. Some bNAbs have evolved to include conserved glycans as part of the epitope[48-51]. Moreover, these surface glycans are also critical for Env folding, viral assembly, and infectivity. Given the overall importance of the Env glycan shield, understanding its molecular architecture and dynamics as a whole is critical for Env-based vaccine design.

The glycosylated Env proteins further undergo additional processing in terms of α-mannosidase and glycosyl transferases; the latter modifies the oligomannose into complex sugars[51]. The level of processing of a particular glycan varies depending on its spatial location, local protein content, local crowding by other glycans, and the producer cell type. A high degree of processing is an indication of exposure or accessibility of sugars to enzymes. At regions with dense crowding of glycans, steric constraints limit the activities of the carbohydrate processing enzymes[52, 53] as the proteins fold and translocate through endoplasmic reticulum and Golgi apparatus. This results in glycoform heterogeneity, and leads to additional problems for structural studies, particularly X-ray crystallography. Thus, most structural studies have so far been performed either by expressing all the glycans in the high-mannose form, or by removing majority of the glycans. Recently there have been a few cryo-EM and X-ray structure determinations of natively glycosylated Env[54-56], however in these structures most of the glycans are not visible beyond the core glycan stem, unless stabilized by interactions with bound antibodies. Similarly, while a number of structural studies have been performed on the HIV-1 Env glycosylation using computational methods, all of these comprise of oligomannose glycan moieties ranging from mannose-5 to mannose-9[18, 35-37, 57]. Here, we have modeled the natively glycosylated Env, having both oligomannose and complex glycans[7, 58]. To our knowledge, this is the first time that a complete computational model of Env SOSIP was generated having native glycosylation pattern including processed glycoforms, thus obtaining results which are physiologically and immunologically more relevant.

Using the natively glycosylated Env trimer of BG505 SOSIP, we have employed graph theory to capture the glycan shield topological network, pinpoint potential interaction pathways, and identify concerted behavior of the glycans. The glycan-glycan and glycan-protein interactions influence the behavior of the shield as a whole and can affect distant sites in the glycan network[7, 18, 35]. Such effects can be captured by this graph-based approach. Analyses of various network attributes, such as relative centrality of different glycan positions and critical subnetwork properties, have aided in detailed examination of the native glycan shield in the context of bNAb interactions. Important global and local feature differences due to native-like glycosylation pattern come to light as compared to all high-oligomannose glycans. We have also been successful in quantifying the glycan shield based on the number of sugar heavy atoms encountered over the antigen surface that can be implemented to define regions of relative vulnerability and regions where the glycan shield blocks access. This information can be incorporated into immunogen design strategies. Due to the rapid yield rate of this method, it can be carried out for a large number of diverse HIV-1 sequences, or can be seamlessly extended to model glycan shields of other viruses.

Results

Selection of site-specific glycans for native glycosylation of HIV-1 Env

The soluble, recombinant BG505 SOSIP.664 (here on referred simply as BG505) trimer has been well characterized as a native-like, Env-mimetic model, and serves as the prototypical immunogen in several vaccine development programs[59, 60]. For our study, we have used this system in the pre-fusion closed conformation, for which several structures have been determined[18, 54-56]. A single protomer of this BG505 protein contains 28 N-linked glycosylation sites. While all N-glycans share a common core sugar sequence, they are broadly classified into three types (**Figure 1A**): (i) oligomannose, in which only mannose residues are attached to the core; (ii) complex, in which differently branching “antennae” are attached to the core; and (iii) hybrid, which is a mix of the first two types. Recent novel mass spectrometry (MS)-based approaches have been successful in identifying site-specific glycosylation profile

in multiple HIV-1 trimers[58, 61]. It is known that each glycosylation site at BG505 has a distribution of multiple possible glycan species, depending on various factors, such as type of cell lines, purification methods and sources, structural constraints, and so on. We used a site-specific distribution of glycan type at each PNGS that was obtained by Behrens *et. al*[7] and Cao *et. al.*[58], to identify the most likely glycan species at each site. The glycan chosen at each site is given in **Supplementary Table S1**. Here we selected the particular species with the highest relative abundance per the MS studies (Figure 1 in reference 7). The structure schematic for each of the selected glycan species have been shown in **Figure 1B**.

Atomistic modeling of the native glycan shield

Due to the highly dense glycosylation on Env surface, an approaching antibody generally requires to navigate through the barrier of sugars to form interactions with the underlying protein epitope. In the static pictures as obtained from fully glycosylated structures[18, 54] and even single snapshots from computational models, a significant fraction of the protein surface appears to be exposed, with each glycan taking up a particular conformation (**Figure 2A**). However, due to their flexible and dynamic nature, these glycans are not confined to a particular conformation, instead sampling a large volume in space. A previous simulation study suggested[62] that the root mean squared deviations (RMSD) for the carbohydrate regions are more than 4 times larger than that of the underlying protein loops. As a result of this conformational variability, the cumulative effect of the glycans over time is like that of a cloud of glycan atoms that shield the underlying surface from any approaching protein probe (an antibody for example) as illustrated in **Figure 2B**.

We have modeled this entire glycan shield with its extensive conformational sampling, over the Env protein. Details of the modeling protocol has been established previously[38] and is reiterated briefly here. A robust ensemble of BG505 glycoprotein 3D conformations in atomistic detail was generated by utilizing a template-free glycan modeling pipeline including a sequence of refinement steps with restraints to enforce proper stereochemistry. The underlying protein scaffold was built by homology modeling from available structures. The glycans were modeled *ab initio* by implementing the ALLOSMOD[63, 64] package of MODELLER[65, 66] in a streamlined pipeline. **Figure 2A** shows a single such pose of the BG505 glycoprotein. Due to the initial

randomization of the glycan orientations, this integrated technique can sufficiently sample a physiologically relevant conformational space accessible to carbohydrates, in a very short time. The complete ensemble has been depicted in **Figure 2B**, which shows that the extensive landscape sampling of the all glycans leads to the overall spatial shielding effect.

The individual glycans modeled by this method covers a biologically relevant landscape. The PNGS asparagine chi1 dihedral, as well as the phi and psi dihedral distributions of 9 different inter-glycan linkages within the ensemble was compared with those obtained from different glycan structures available in the PDB database, as described in **Supplementary Figure S1**. The torsion angle distributions from the PDB were obtained using GlyTorsion webserver[67]. These distributions match very well between our generated ensemble and the PDB structures, as demonstrated in details in the Supplementary Information. We had previously built a similar ensemble with mannose-9 glycans at all glycosylation sites[38], and had validated this method for ensemble generation by quantitatively comparing the mannose-9 models to cryo-EM data from oligomannose-predominant BG505.SOSIP.664 Env structures utilizing progressive low-pass filtering[38]. That study confirmed that our methodology for characterizing the structural and dynamical properties of the glycan shield accurately captures the properties of the physiological ensemble. In this current study, we used the same ensemble (hereon referred as all-man9 model) for comparison to understand the effects of native glycosylation.

Influence of complex glycans on glycan shield

Glycan dynamics, type, and inter-glycan interactions determine the local shielding effect over the Env protein. Here, we looked at the dynamics of individual glycans and how they change due to native-like glycosylation, ultimately governing the glycan shield properties. Each glycan samples a large region in space as shown in **Figures 2C** and **2D**. These fluctuations of course become much more extensive, when the glycans are present on the variable loops, due to the dynamic movement of the protein backbone of the loops at these regions. The root mean squared fluctuations (RMSF) measure and the sampled volume for those glycans located on the loops are generally much higher, as seen in **Figure 3A** and **Supplementary Figure S2A**. However, aligning the protein backbone and considering the reduced RMSF contribution coming only from the glycans (see Methods), we see that the fluctuations between different glycans are comparable, with

a maximum difference of ~1.5Å (**Supplementary Figure S2B**). As for the glycan specific sampled volume, after removing the flexibilities brought on by protein loop motions, the glycans on and flanking loop V2 and those in gp41 cover the largest regions in space (**Figure 3B**).

Considering the differences between native-like glycosylation and the all-man9 model, some interesting consistent patterns emerge. Comparing the reduced RMSF between native and all-man9 glycosylation in **Figure 3C**, we see that while glycans 88, 355, 398 and 406 have decreased fluctuations in the native model, those of glycans 234, 462, 611, 618, 625 and 637 have increased significantly. With the exception of 234, all of these glycans are complex sugars. The presence of the charged sialic acid at the tips of almost all of these complex glycans can dictate the interactions between neighboring glycans, increasing their structural variations if surrounded by other charged glycans, or reducing them if a stable conformation buried between uncharged high-mannose patches can be found. The man-9 glycan at N234 itself is centrally located between a number charged glycans, those at 88, 462, 625 and 637. The high fluctuations of this glycan can stem from its attempt to screen these neighboring negatively charged sugars. The complex sugars in gp41 (611, 618, 625 and 637) have also been shown to have high variations in cryo-EM maps[68]. The total volume sampled is generally larger for native glycosylation, compared to the all-man9 model (**Figure 3D)**. This is not unexpected, since complex glycans generally have larger number of sugars, including the bulky fucose ring at the base. The centrally located high-mannose patch has almost similar volumes in both the models.

Another important difference in models that include complex glycans versus the all-man9 model results from the presence of the fucose ring at the core of the complex glycans (**Supplementary Figure S2C)**. By structurally aligning the first core sugar and the three residues at the base of the glycan (n-1, n, n+1; where n is the glycosylated asparagine residue) for all the structures in the ensemble, the oligomannose glycans are found to be spaced symmetrically around the core, while complex sugars have a distinct bend away from the side where the fucose ring is present. This difference in orientation preference, along with the presence of the negatively charged sialic acid tips of the antennae, play notable roles that govern the differences between high oligomannose and native glycosylation of the Env. A close examination of the high-threshold difference maps generated in our previous study[38] also reveals such changes in dynamics around single glycans. For instance, the cryoEM map intensity difference around the complex glycan at

N618 is located primarily on the underside of the glycan stalk, facing the body of the RM20A3 Fab, suggesting that complex type glycans can interact weakly with the Fab in a way high-mannose type glycans cannot. A change in projection angle relative to the peptide surface can also lead to a difference signal; for example the difference signal around the glycan at N611 is strongest below the glycan stalk supporting the hypothesis that a change in glycan projection angle can add asymmetry to the glycan stalk and could affect its dynamics.

Network analysis of glycan topology explicates the shield connectivity

The BG505 trimer, like all HIV-1 Envs, has a highly dense glycosylation pattern and each glycan sample a particular region in space (**Figure 2D**), such that neighboring glycans can occupy overlapping regions (**Figure 4A**). The fraction of volume overlap gives a measure of the interaction probability between the constituent glycans. **Figure 4B** shows a heat map of the glycan-glycan volume overlap within a protomer, while **Figure 4C** represents inter-protomer overlap. Within a protomer there are three main regions of overlap – the apex, the gp41 base, and the glycan-dense central high-mannose patch. Inter-protomer overlaps are mainly due to V1 and V2 loop glycans near the trimer apex.

While each glycan exerts effects in its immediate vicinity, due to the inter-glycan interactions, their influence can percolate over long distances across the surface of protein. Long-range glycan interactions can occur, as with perturbation of a glycan at one site can affect the processing and antibody interactions of another glycan at a distant site[7, 18, 23, 69]. Understanding long-range interactions between glycans is important for characterizing global properties of the glycan shield. We employed graph theory to describe the glycan shield topological network and to examine if this network can successfully capture the long-range interactions.

Network analyses has historically been used to study protein allosteric frameworks and evolutionary paths [70-74], and only recently has begun to be applied to in glycoprotein structural characterization [37]. We have previously established this graph-based method, where the network from all-man9 model was verified against cryo-EM data[38]. High network degree correlation with per-glycan map intensity, and centrality correlation with progressive enzymatic digestion of

glycans affirms the strength of this network-based approach to capture the shield topology accurately. Detailed methods of modeling the network are recapitulated in the Methods section. Our network is based on a combination of intra and inter-protomer glycan volume overlap maps (**Figures 4B** and **4C)**. **Figure 5A** shows the obtained network of BG505 native glycosylation unfolded and laid out in 2 dimensions for the ease of visualization. This is a force-directed layout, which uses attractive forces between adjacent nodes and repulsive forces between distant nodes to reach an optimum distribution of the node points in space[75]. **Supplementary Figure S3** gives another representation of the network with respect to the BG505 structure.

The overall topological features remain the same as the all-man9 network described in our previous study[38]. The nodes in the central region around the V4 loop, in the high-mannose patch, are very highly inter-connected. Glycans in the V1, V2 apex are also reasonably well-connected, but the connections at the base near gp41 are relatively sparse, both within the locality, and globally with the rest of the network. Glycans at positions 355, 462 and 276 connect the sparse base region of the network with the dense apex and central regions. Glycan 160, and those in the V2 loop, enable inter-protomer glycan interactions at the apex, stabilizing the protein quaternary trimer structure[38]. Glycan 197, crucial in the binding of CD4bs and V3-specific antibodies[57, 76], connects the central crowded region of the network between neighboring protomers. gp41 glycans 611 and 637 also contribute to inter-protomer pathways, with glycan 637 communicating with glycan 448 directly in the central mannose patch.

Utilizing the glycan graph to extract functionally relevant topological features

The degree of a node in a network is the number of connections it has to other nodes (**Figure 5B**). The native glycosylation network is well-connected. Due to the high structural fluctuations of the V2 loop, the glycans on and flanking V2 can interact with a number of other neighboring nodes, having the highest degrees of connectivity. There is dense crowding of glycans around the high mannose patch with a number of inter-connections, resulting in the glycans of this patch being less processed because of reduced accessibility to enzymes[52, 77, 78]. The network degree values are the lowest around the base of the protein on and around gp41, reflective of the sparse architecture of glycan topology in this region.

While the shield is a result of the cumulative effect of all the glycans, the importance of each of these glycans is not uniform. To elucidate the relative influence of each of the glycans on the network, we calculated the eigenvector centrality, or eigencentrality, of the nodes to measure its connectivity to the network. A large relative value indicates that the node is well connected to the network and thus is "centrally" located, whereas a low relative value indicates that the node is on the periphery of the network. Operationally, the eigencentrality is the eigenvector associated to the largest eigenvalue of the adjacency matrix, that in position (i,j) reports the overlap of the ensemble of glycan at sites i and j. That value will be zero if the glycans in position i and j do not physically interact (details given in Methods section). The normalized eigencentrality of the glycans are projected on the network as a colormap in **Figure 6A**. The eigencentrality increases towards the middle of the graph, with the glycans at the crowded central patch with a large number of connections between each other having the highest centrality values. When we increase the threshold of volume overlap needed to form an edge, those glycans with the least centrality leave the network first. Glycan 611 is the first to be eliminated, succeeded by some of the inter-protomer interactions and the other gp41 glycans, following the relative centrality scores. The core patch of glycans with high eigencentrality values, mainly consisting of high-mannose glycans, persist throughout the subnetwork.

We have previously shown[38] that successive enzymatic digestion of glycans from Env follows a pattern that matches with the network centrality. Those glycans which are sparsely connected to each other, having lower centrality, are eliminated earlier during the process of endoH digestion. On the other hand, the glycans having higher network centrality, such as those in the high-mannose patch, takes longer to be eliminated by the digestive enzymes. The eigencentrality calculated from the all-man9 network and localized intensities after two hours of endoH digestion (Figure 8, reference [38]) have a Pearson's correlation coefficient of ~0.8, and a p-value of 1.14e-05. Thus the eigenvector centrality provides a quantitative measure of the crowding of the highly central glycans that makes them difficult to access for stripping off by endoH action. This comparison with experiments gives compelling evidence of the validity of the network.

Next, we calculate the shortest paths between any two sites on the glycan interaction network. As an example, **Figure 6B** shows the shortest paths to all glycans from the glycan at site N332. The site N332 is central in the glycan interaction network, and is known to have both direct

and subtle long-range influences over a number of bNAb sites[7, 69]. Our calculation shows the most probable pathway over which each glycan feels the influence of the glycan at site N332. The shortest paths were calculated using the Floyd-Warshall algorithm[79, 80], where the inter-glycan distances were edge-weighted.

Influence of complex glycans on overall network topology

The degree of connectivity decreases almost throughout the network for the native glycosylation (**Supplementary Figure S4A**). The number of stable glycan-glycan interactions at several glycan sites decreases because spatially proximal glycans avoid unfavorable charge-charge interactions. For example, the uncharged glycan 234 takes up a position central to all the neighboring charged sugars, increasing the distances between them, and the charged N406 glycan buries itself in the middle of the surrounding high-mannose glycans (**Figure 6A**), clustering together with them. In fact, removal of this charged glycan N406 glycan can increase the processing of the neighboring high-mannose moieties[81]. This can result from breaking down of this clustering of glycans, leading to increased accessibility by glycosyltransferases and other glycan-processive enzymes. A decrease in connectivity slightly increases the overall diameter of the native network, increasing the mean number of hops for the shortest path from 2.4 hops (and distance 0.19) in the all-man9 model to 3 hops (and distance 0.27)

The distribution of centrality also shifts between the two models (**Supplementary Figure S4B**). The centralities of the V1 and V2 glycans, along with those at 197, 234, 276 and 462 increase due to native glycosylation. On the other hand, the high-mannose glycans present in and around V3 region decrease from the all-man9 model. **Figure 7A** illuminates the difference in adjacency matrices between the two models, with blue color indicating at least 5% decrease in edge weight, and red indicating at least 5% increase in edge weight in native network, as compared to all-man9. Overall connectivity goes down in the apex and the central patch for the native, and increases within gp41 glycans, as compared to all-man9. The differences between the two networks are shown in **Figure 7B** and **C**. The pathways 137 to loop V2 glycans and 332 as well as those between 355 through 625 to 618 become stronger in native glycosylation. A new connectivity comes up between 197 and 276, and a number of paths starting from 197 become shorter (**Figure 7B**). Some of these 197 connections, such as those with 276 and the V5 loop glycans occur across the CD4

binding site. It was previously shown that in predominantly high-mannose Env structures, CD4bs targeting antibody VRC01 has very little interaction with glycans 197 and 276[18]. Conversely, in another Env structure with fully processed native glycans, a VRC01-like antibody called IOMA interacted extensively with both 197 and 276[54]. This matches our observation of increased orientation of glycan 197 over the CD4bs in native glycosylation pattern. However, the paths connecting 137, 156, 301, and 197 (of neighboring protomer) are significantly weakened in the native model (**Figure 7C**). Two other subnetworks involving V1,V2 loop glycans and the central mannose patch become weaker due to the presence of native glycans.

Quantifying the vulnerability of glycan shield for antibody-based neutralization

To capture the impact of the glycan shield acting as an immunological barrier, we quantified the sugar barrier over the Env protein surface using the ensemble of structures that have been generated. Towards this goal, we have defined the glycan encounter factor (GEF) to be the number of glycan heavy atoms encountered by an external probe approaching the protein surface. This factor is calculated at each residue on the surface of the protein within a probe of diameter 6Å calculated using our ensemble. The highest value obtained is 12 for the native model, and is located in the HMP. Based on existing structures, the main interaction points between Env and bNAbs are often hairpin-like loop regions. Even large-scale atomistic simulations suggest that the first line of contact between Env and an antibody is through a peptide loop[82]. Accordingly, for our analysis, we have used a probe size of 6Å, which is the typical diameter of a hairpin loop. At each residue present on the surface of the protein, the approaching probe was considered in three directions (**Figure 8A**): perpendicular to the surface **z**, and then the **x** and **y** directions spanning the plane parallel to the surface. The geometric mean of the three values were taken to get the final GEF per residue on the Env surface. This value will go to zero when the glycan encounter factor is zero from any one of the three cardinal directions. Thus, for any point on the surface which has a dense glycan covering, such as D in **Figure 8B**, has a high glycan encounter factor value, versus a point such as R where the glycan covering is sparse, which will have a low GEF.

Figure 8C shows normalized GEFs mapped onto the trimer protein surface (**Figure 8C**). Previous evidence suggests that 70% of the Env ECD surface area is covered by glycans[45]. Based on this, we determined the lower cut-off of GEF below which we can define glycan holes.

The calculated solvent-exposed surface area of the protein part of our modeled BG505 structure without considering glycans is 86,055 Å^2. Excluding the exposed region at the base of the soluble SOSIP, this reduces to 79,672 Å^2. Varying the lower cut-off of GEF, we find that a cut-off of 1.5 GEF leads to 30% of the surface to be exposed. Regions of BG505 surface having a GEF less than 1.5 is colored in black in **Figure 8D**. From the figure, it is clear that the typical glycan holes targeted by bNAbs in BG505, such as the CD4 binding site, the V3-loop epitope and the fusion peptide binding region fall below this GEF cut-off. GEF tracks with epitopes that are relatively generic to a broad range of Env strains[83, 84].

Antibodies elicited by BG505.SOSIP.664 are mainly biased towards the missing 241 and 289 glycan hole (GH) and the cleft-of-trimer (COT) epitope regions as demonstrated by cryo-EM and immunogenicity assays[85, 86] (see Figure 1 in reference [86]). The GEF parameter identifies these BG505-specific eptiopes as breaches in the glycan shield (**Figure 8B**, "R" region; **Figure 8D** yellow dashed circle). On the other hand, the densely glycosylated regions around V2, V4 loop and alpha 2 helix have high values of GEF. At each point, the GEF value is given by a combination of all glycans in the vicinity that can come in the way of the approaching probe. At the same time, we can analyze the extent of influence of each glycan on the protein surface. Thus, GEF calculations could aid in interpreting Env sensitivity profiles to bNAbs, and for estimating the impact of interactions of glycans with in the network on epitope exposure for immunogen design. And we are now equipped with a tool to quantify the barrier effect of the glycans individually or as a group, as further demonstrated[85, 86] in the following section.

Combining network topology and glycan encounter factor to inform on local and global effects of neutralization

To better understand the dynamics of the glycan shield in the context of neutralization by bNAbs, we examine the clustering of glycans within the network. We define communities using a modularity maximization approach that divides the network into sub-modules or groups (see Methods). Communities have dense connections between the nodes within a module and comparatively sparse connections between nodes in different modules (**Figure 9A inset**). This analysis identifies five distinct communities within the BG505 native glycan network (**Figure 9A and B**). The apex glycans around loop V2 from the three protomers together form a single

community (1, green). Right below that, glycans 137, 262, 295, 301, and 448 (2, blue) forms a community around the V3 and alpha 2 helix. Glycans 133, 197, 363, 386 and 392 (3, yellow) and 339, 398, 406 and 411 (4, red) form two distinct communities involving the glycans on and surrounding V4 loop region. The rest of the glycans with 88, 234, 276, 355 and 462 from gp120 and all four glycans from gp41 form the fifth community (5, cyan), though the modularity value is lower due to sparser connections. While the glycan shield is well connected even between the communities, the glycan-glycan interactions within each community is much higher. The possibility of an approaching probe reaching the protein surface through these strongly connected communities is low. A similar study clustering glycans from microsecond simulation runs of BG505 SOSIP was performed by Lemmin *et. al.*[37], identifying 4 glycan microdomains that roughly correspond to our modules 1, 2, (3+4) and 5. However, in that study, mannose-5 glycoform was used at all sites, and due to the smaller length of these glycans, some of the interactions, including inter-protomer interactions were not observed. Remarkably, in that study, junctions between microdomains were found to indicate regions of relative vulnerability. The communities we identified, also demarcate the regions where the glycan shield can be penetrated. Broadly neutralizing antibodies whose binding epitopes are known target these community boundaries (**Figure 9A**). Thus, glycan community dynamics can help to determine susceptible regions of the glycan shield, and can be further used for guiding immunological studies.

The proposed network is useful in deciphering the impact of addition or deletion of glycan on neutralization. Removal of the high conserved glycan at 197 by mutating the sequon leads to enhanced neutralization sensitivity to a variety of CD4bs and V3-specific antibodies[76, 87, 88]. This glycan is situated proximal to the CD4 binding site, and the tip of V3 loop, directly affecting the binding of these antibodies. However, past experimental evidence also suggests that the deletion of this glycan at N197 increases the binding affinity of two antibodies PG9 and PGT145 [7] which target the trimer apex of Env. The epitope of PG9 as determined from the PDB structure 5VJ6 include residues 160, 161, 167-173, 185, 305 and 307 (**Figure 10A**) and the epitope of PGT145 as determined from PDB structure 5V8L include residues 123, 124, 127, 160-162, and 167-169 (**Figure 10A**). The footprint of glycan 197 as per our GEF model is shown in **Figure 10B**. Residues of the antibody epitopes do not overlap with those regions directly covered by glycan

197. Yet, removal of glycan 197 results in significant reduction in the glycan encounter factor over the V2 antibody epitope as evidenced in **Figure 10C** and **D**.

The removal of glycan 197 affects the glycans that were originally acting as barriers over the epitopes to resample the available space in such a way that the barrier over the epitopes is now reduced. Glycans 156, 160, 185e and 185h from the neighboring protomers directly shield the PG9 and PGT145 epitopes. Looking at the shortest paths of communication between residue 197 from either of the protomers to all other glycans (**Supplementary Figure S5A and S5B**) demonstrate that while glycan 185e interacts with glycan 197, other glycans covering the epitope regions communicate with 197 via a series of inter-glycan interactions. Deletion of 197 does not only affect the V1/V2 loop region glycans. The difference in adjacency matrix due to this perturbation is illustrated in **Supplementary Figure S6**. Interactions such as those between glycans N133 - N386, N295 – N406, N398 – N339, and N411 – N448 are reduced more than 10%. On the other hand, glycan 276, which was originally interacting strongly with 197 now forms new interactions with N295, N332 and N411 and N448 glycans. Therefore, deletion of the glycan at 197 also causes significant changes to the shield topology up to the V4 loop region, and our methodology describing the glycan shield network corroborates the experimental findings, and sheds light on the most probable pathways through which the glycan-glycan communications occur.

Discussion

The dense arrangement of N-glycans masks antigenic surfaces on Env, acting as a dynamic shield protecting the protein from the adaptive immune system. Moreover, since host proteins have similar glycosylation pathways, these self-glycans are generally immunologically inert. Understanding the structure and dynamics of the glycan shield as a whole is therefore important for Env-based vaccine design. While X-ray, NMR and cryo-EM structures have supplied a number of important molecular details about the Env glycoprotein, they do not account for the high flexibility and dynamics of these glycans that leads to the glycan shield. Detailed characterization of the glycan shield and the quantification of the resilience and vulnerability of this barrier over the Env surface can add new perspective and depth to current HIV vaccine design efforts.

All previous computational studies have generalized glycan moieties as simple oligo-mannoses such as mannose-5 and mannose-9 [18, 35-37, 57] for the purpose of modeling. For the first time, we have incorporated native glycosylation, and included complex sugars based on site-specific mass spectrometry results. While the overall glycan aspects of the network are consistent between mannose-9 and native-like glycosylation, there are critical differences. The most noteworthy are a consequence of the presence of the bulky fucose ring at the base or the negatively charged sialic acids at the antennae tips. These lead to overall rearrangement of glycan orientations affecting its microenvironment, and ultimately influencing the shield topology. Thus, our comprehensive view of the shield is capable of capturing individual glycan effects which are physiologically and immunologically more relevant.

Our network-based approach enables in understanding the collective behavior of the glycans. We can compare the relative centrality of glycans, and identify potential interaction pathways. Importantly, the centrality or importance of glycans correlates well with experimental cryo-EM data[38]. Glycans with lower centrality have lesser influence on the graph, and are the first to be eliminated from the network, if the adjacency threshold is increased. At the same time, the most central region of the network is the most resilient to enzymatic action. Such centrality measures can help determine the ease of targeting glycans and their modifications, guiding the process of immunogen development in the context of distinct Envs.

Complex networks of glycan interactions that give rise to long range effects over the shield topology are evident[7]. We have also identified specific communities of glycans in the shield that have high degrees of interaction within each community. The antigen surface under each such community is therefore better shielded, and the regions under community junctions are more susceptible to antibody binding. The boundaries of such glycan domains have been previously identified to be regions of vulnerability[37]. While the shield resilience is the main consideration for epitope exposure, some antibodies have also evolved to capitalize on specific interactions with a number of the conserved glycans during their molecular engagement with the epitope. Due to the stability of glycan interactions within the communities, the community detection can also aid in the determination of antibody angle of approach that has been shown to influence the breadth of bNAbs [89].

There are known common and uncommon 'holes' that can open up in the shield to make the virus more vulnerable, or conversely get covered resulting in immune escape, as a result of evolutionary addition/deletion or shift of glycans[22]. Previous advances have been made in identifying breaches in the shield based on the area of influence of each glycan[22]. In this study, we have found that this area can vary, depending on the glycan type, charge, neighbors, etc. Amino acid signature analyses suggest that even minor perturbations such as single site mutations could potentially change the shielding effect over certain epitope regions[69]. Therefore, we have derived a measure to quantify the shielding effect based on the encounter factor of glycan over the antigenic protein surface. This tool allows us to define regions of relative vulnerability and resilience in the glycan shield.

The method we developed here for the structural modeling of the glycoprotein atomistic ensemble and the subsequent development of the network is high-throughput compared to traditional sampling by MD simulation methods. Due to the ease of this fast and efficient pipeline we are now equipped with a tool to perform comparative structural studies due to glycan additions, deletions or modifications, as well as other variations in the Env protein. This is important to understand the evolution of the glycan shield over longitudinal sampling of lineages. The structural basis of addition or removal of glycans that are known to drive antibody maturation and neutralization activities[90, 91] can also be easily investigated utilizing this pipeline. Capitalizing on the relatively low computational overhead of this approach, our pipeline can be integrated into a polyclonal epitope mapping assay to track the glycan shield as a function of hierarchical antibody response, by modeling the shield network with the presence of different antibodies and observing how the topology is altered.

While this approach captures the equilibrium ensemble of glycan spatial distribution, it lacks temporal information regarding the glycoprotein dynamics and any topological transitions that might occur on shorter timescales. Computationally costly MD simulations could potentially address the dynamics of hierarchical glycan topology. These simulations can also provide insights on how antibodies navigate the transient accessibility of epitope through highly flexible glycans and to refine the 6Å probe considered here.

Beyond HIV-1 and other viral envelope proteins, the significance of glycoproteins in a vast array of biological processes from protein folding, cellular communication to immune-regulation, make them a fast-emerging field of interest in biomedical research. Changes in these glycosylation patterns have been associated with various diseases, including rheumatoid arthritis[92], and cancers[93]. Additionally, many of the current therapeutic antibodies in the market are N-linked glycoproteins, and the significance of N-glycans is becoming increasingly evident [94]. The ease of modeling of glycan network utilizing our approach makes it translatable to other systems, and can assist in determining the role of these glycans in conjugation with the underlying proteins at a molecular level. In comparison to N-glycans, our understanding of O-glycosylation is limited. This class of glycans are relatively more complex in terms of structural variations. It would be an interesting challenge to generalize our methodology to encompass O-glycosylated systems as well, that are present to some extent on HIV-1 Env. This can also help gain molecular insights on such refractory systems, like Ebola that have both N- and O-linked glycosylation, and in understanding the pathological implications of dense O-glycans in mucin associated cancers[95].

Because of its chronic persistence in infection, HIV and the human immune system are at war constantly, and the virus uses the Env glycan shield to mask the human immune surveillance. One battlefront in this war is the glycan shield: while the virus evolves to develop resilience, the immune response counteracts by looking for vulnerabilities. As efforts are underway to aid the immune system overcome this race by conditioning it with engineered immunogens, there is a need to quantify the resistance and vulnerability of glycan shield in a more quantitative manner. This is that first time that the native glycan network and shielding has been spatially quantified. Our derivation of the Glycan Encounter Factor measures the relative barrier over the Env surface, and can potentially aid to distinguish subtle differences on the shield due to variations in the glycosylation or even protein sequences. We are therefore armed with a set of *in silico* tools with which to help the anti-HIV war efforts and guide immunogen design.

STAR Methods

Contact for Reagent and Resource Sharing

Further information and requests for resources and reagents should be directed to and will be fulfilled by the Lead Contacts Andrew B. Ward (andrew@scripps.edu) and S. Gnanakaran (gnana@lanl.gov).

Method Details

High-throughput conformational modeling

The ensemble of BG505 glycoprotein 3D conformations were built in atomistic detail by implementing the ALLOSMOD[63, 64] package of MODELLER[65, 66]. The BG505 protein scaffold was homology modeled, by threading the protein sequence into available crystal structure templates. SOSIP structure with PDB accession ID 4ZMJ[96] was used as the template for gp120, that also guided the three-fold symmetry of the trimer. 5CEZ[97] was used as the template for gp41 and since it has the least number of missing residues among the available structures. The missing residues in the loops were modeled *ab initio*, using known disulphide bonds as additional restraints. 100 protein models were generated, and the best 10 were selected as starting scaffolds for glycan building, based on MODELLER optimization scores, and stereochemistry scores as determined by PROCHECK[98]. This results in different starting orientations of the hypervariable loops. For each of the 10 selected protein structures, glycans were initially added with random orientation, at the known glycosylation sites, based on ideal geometries as dictated by CHARMM36[99, 100] force field internal coordinates, followed by a 1Å randomization added to the overall atomic coordinates as described by Guttman et. al.[64]. Once all the glycans were added, ensuing refinement steps of the glycoprotein system optimized an energy function given by a combination of template-based spatial restraints, CHARMM36 forcefield terms, and a soft sphere-like truncated Gaussian term to prevent collisions. The structures were relaxed with 1000 steps of conjugate gradient minimization followed by a short molecular dynamics equilibration of 500ps. Further refining with five rounds of simulated annealing was performed between 1,300K to 300K in 8 steps. The glycans and the loop regions were kept flexible during the refinement steps. 100 fully glycosylated structures were modeled from each of the 10 selected protein models,

resulting in the final ensemble containing 1000 different poses. In order to let these unstructured loops sample a wider range of conformations, we removed the template restraints from these loop regions during the protein homology modeling phase. These residues by HXB2 numbering are as follows: 143 to 152 (V1 loop), BG505-specific insert residues 185A to 185I and 186 to 189 (V2 loop), 309 to 315 and 325 to 329 (V3 loop), 400 to 410 (V4 loop) and 458 to 464 (V5 loop) as determined from the LANL HIV database (https://www.hiv.lanl.gov/).

Glycan root mean square fluctuations

For both the native and all-man9 glycosylated models, the root mean square fluctuations (RMSF) of each glycan (with index *n*) was calculated as an average over all its heavy atoms, by the following equation:

$$RMSF_n = \frac{1}{K}\sum_{k=1}^{K}\sqrt{\frac{1}{M}\sum_{m=1}^{M}|\vec{r}_{mnk} - \langle\vec{r}_{nk}\rangle|^2}$$

where $\vec{r}_{mnk}$ is the atomic position of heavy atom k of glycan n in snapshot m, $\langle\vec{r}_{nk}\rangle = (\frac{1}{M})\sum_{m=1}^{M}\vec{r}_{mnk}$ is the average atomic position of heavy atom k in glycan n. K is the total number of heavy atoms in the glycan. It is 127 for man-9, and varies depending on the type of glycan. The ensemble for each model contains 1000 snapshots, making M = 1000 snapshots for each of the two models. The standard deviations (s.d.) were obtained by dividing the 1000 snapshots into 4 sets of M=250, and calculating the four sets of RMSF values (Figure 3A).

The 1000 structures of the total ensemble are built from 10 initial starting protein conformations, as described above. The main difference between these 10 conformations are the variations in the loop regions, due to the missing residues in the templates. In order to reduce the effects of the loop fluctuations and consider the RMSF coming from the glycans alone, the reduced RMSF values were also calculated in each of these 10 sub-models, and their average and s.d. calculated (**Supplementary Figure S2B**). The RMSF difference between the models (Figure 3D) were obtained by subtracting the reduced RMSF values of all-man9 from native model (native minus all-man9). Since, the average reduced RMSF value is ~4Å, only those RMSF difference

values are statistically significant which are above 0.2 Å, which corresponds to a p-value of 0.05, rejecting those values within the null hypothesis.

Glycan volume overlap and network analysis

The inter-glycan overlap is calculated as the total fraction of heavy atoms from the two glycans that come within 5Å of each other. Let us consider the example of mannose-9 to illustrate the parameter of overlap. A single mannose-9 glycan has 127 heavy atoms. Since our ensemble is composed of 1000 possible structures, there are effectively 127,000 heavy atoms per ensemble of mannose-9 at one position. The fraction of the total number of heavy atoms from two neighboring ensembles that come within contact distance defines the overlap fraction. Since mannose-9 is the most commonly occurring glycoform in our system, we have used it as our reference for normalization of the overlap probability. An overlap greater than or equal to 50% of heavy atoms from two neighboring mannose-9 glycans is assigned as 1. This overlap matrix is used to define the adjacency matrix for our network analysis. Each glycan functions as a node of the graph (Figure 5A inset), and two nodes are connected by an edge if there is at least 5% overlap as per our overlap definition given above. The edge length is inversely proportional to the overlap value, i.e., the larger the overlap, the closer two nodes (glycans) are in the graph. Only those glycans from the neighboring protomers are considered, that have an inter-protomer edge. All graph theory and network analyses were performed using Python[101] and Matlab_R2018a packages[102].

Eigenvector centrality calculation:

For a given graph, G, with adjacency matrix $\mathbf{A}=(a_{v,t})$ where $a_{v,t}$ is the edge weight connecting nodes v and t ($a_{v,t}=0$ when there is no connection), the relative centrality score x, of node v can be defined as:

$$x_v = \frac{1}{\lambda} \sum_{t \in N(v)} x_t$$

where $N(v)$ is the set of neighbors directly connected to v, and λ is a constant. From the definition of the adjacency matrix where the elements go to zero if two nodes are not connected, the above equation can be expressed as:

$$x_v = \frac{1}{\lambda}\sum_{t \in G} a_{v,t} x_t$$

This has the form of the eigenvector equation **Ax**= λ**x.** With the added constraint of the eigencentrality values needing to be non-negative, by the Perron-Frobenius theorem[103], the eigenvector corresponding to the largest eigenvalue gives the desired measure of centrality. The eigenvector is a unit vector and therefore the centrality values add up to one. For the purpose of this work, we have normalized the centrality values with respect to the node with the highest centrality assigned at 1, to obtain the relative centrality values.

Modularity maximization for community detection

Community detection within the glycan network was performed using the modularity maximization approach given by Newmann and Girvan[104, 105]. Modularity Q is calculated as the difference between the fraction of edges that fall within a module and the expected fraction if the edges were distributed in random.

$$Q = \sum_{i=1}^{k} (e_{ii} - a_i^2)$$

Where e_{ii} is the fraction of edges in module *i*; a_i is the fraction of edges with at least one end in module *i.* It is calculated by a greedy heuristic, beginning with the trivial system of each node being a cluster, and merging two clusters that will increase modularity by the largest value, stopping when any further merge would decrease the modularity. This approach is known to work well for small networks similar to our system. The calculations were implemented through a standard algorithm[106] in Matlab R2018a.

Data Availability

All data needed to evaluate the conclusions in the paper are present in the paper and/or the Supplementary Materials. Additional data related to this paper may be requested from the authors.

Supplemental Information

Supplemental Information includes 6 Figures, 1 Table, and details of torsion angle distributions of modeled glycan structure.

Acknowledgements

S.C., B.T.K and S.G were funded by grants from the NIH (Center for HIV/AIDS Vaccine Immunology and immunogen Discovery, UM1 AI100645; Consortia for HIV/AIDS Vaccine Development, UM1 AI144371). Z.T.W and A.B.W were supported by the National Institute of Allergy and Infectious Diseases grants: UM1 AI100663 and UM1 AI144462, and Collaboration for AIDS Vaccine Discovery (CAVD) grant OPP1115782. S.C was also partially supported by the Center for Nonlinear Studies (CNLS) at Los Alamos National Laboratory (LANL). We acknowledge Timothy Travers and Cesar Lopez for suggestions on glycan modeling, Kshitij Wagh for insights on glycosylation holes in HIV, Kevin Weihe and Rory Henderson from Duke University for helpful discussions on Env immune response. S.C and S.G acknowledge the LANL High Performance Computing Division for providing computational facilities.

Author Contributions

Conceptualization, S.C., Z.T.B, N.W.H., B.T.K., A.B.W. and S.G; Methodology, S.C., Z.T.B, N.W.H., A.B.W. and S.G.; Modeling and Simulations, S.C.; Cryo-EM experiments, Z.T.B.; Formal Analysis, S.C. and Z.T.B.; Visualization, S.C. and Z.T.B.; Manuscript Preparation, S.C., Z.T.B, N.W.H., B.T.K., A.B.W. and S.G.; Supervision, A.B.W. and S.G.

Competing Interests

The authors declare no competing interests.

References

1. An, H.J., J.W. Froehlich, and C.B. Lebrilla, *Determination of glycosylation sites and site-specific heterogeneity in glycoproteins.* Curr Opin Chem Biol, 2009. **13**(4): p. 421-6.
2. Dwek, R.A., *Glycobiology: Toward Understanding the Function of Sugars.* Chem Rev, 1996. **96**(2): p. 683-720.
3. Moremen, K.W., M. Tiemeyer, and A.V. Nairn, *Vertebrate protein glycosylation: diversity, synthesis and function.* Nat Rev Mol Cell Biol, 2012. **13**(7): p. 448-62.
4. Dennis, J.W., M. Granovsky, and C.E. Warren, *Protein glycosylation in development and disease.* Bioessays, 1999. **21**(5): p. 412-21.
5. Stanley, P., N. Taniguchi, and M. Aebi, *N-Glycans*, in *Essentials of Glycobiology*, rd, et al., Editors. 2015: Cold Spring Harbor (NY). p. 99-111.
6. Wang, B., et al., *Mechanistic understanding of N-glycosylation in Ebola virus glycoprotein maturation and function.* J Biol Chem, 2017. **292**(14): p. 5860-5870.
7. Behrens, A.J., et al., *Composition and Antigenic Effects of Individual Glycan Sites of a Trimeric HIV-1 Envelope Glycoprotein.* Cell Rep, 2016. **14**(11): p. 2695-706.
8. Wang, C.C., et al., *Glycans on influenza hemagglutinin affect receptor binding and immune response.* Proc Natl Acad Sci U S A, 2009. **106**(43): p. 18137-42.
9. Nothaft, H. and C.M. Szymanski, *Bacterial protein N-glycosylation: new perspectives and applications.* J Biol Chem, 2013. **288**(10): p. 6912-20.
10. Burton, D.R. and J.R. Mascola, *Antibody responses to envelope glycoproteins in HIV-1 infection.* Nat Immunol, 2015. **16**(6): p. 571-6.
11. Sommerstein, R., et al., *Arenavirus Glycan Shield Promotes Neutralizing Antibody Evasion and Protracted Infection.* PLoS Pathog, 2015. **11**(11): p. e1005276.
12. Zhang, X., et al., *Structures and functions of the envelope glycoprotein in flavivirus infections.* Viruses, 2017. **9**(11): p. 338.
13. Szakonyi, G., et al., *Structure of the Epstein-Barr virus major envelope glycoprotein.* Nat Struct Mol Biol, 2006. **13**(11): p. 996-1001.
14. Lennemann, N.J., et al., *Comprehensive functional analysis of N-linked glycans on Ebola virus GP1.* MBio, 2014. **5**(1): p. e00862-13.
15. Ilinykh, P.A., et al., *Asymmetric antiviral effects of ebolavirus antibodies targeting glycoprotein stem and glycan cap.* PLoS Pathog, 2018. **14**(8): p. e1007204.
16. Amanat, F., et al., *Antibodies to the Glycoprotein GP2 Subunit Cross-React between Old and New World Arenaviruses.* mSphere, 2018. **3**(3).
17. Saphire, E.O., et al., *Systematic Analysis of Monoclonal Antibodies against Ebola Virus GP Defines Features that Contribute to Protection.* Cell, 2018. **174**(4): p. 938-952 e13.
18. Stewart-Jones, G.B., et al., *Trimeric HIV-1-Env Structures Define Glycan Shields from Clades A, B, and G.* Cell, 2016. **165**(4): p. 813-26.
19. Karsten, C.B. and G. Alter, *The HIV-1 Glycan Shield: Strategically Placed Kinks in the Armor Improve Antigen Design.* Cell Rep, 2017. **19**(4): p. 669-670.
20. Ringe, R.P., et al., *Closing and Opening Holes in the Glycan Shield of HIV-1 Envelope Glycoprotein SOSIP Trimers Can Redirect the Neutralizing Antibody Response to the Newly Unmasked Epitopes.* J Virol, 2019. **93**(4).
21. Crispin, M., A.B. Ward, and I.A. Wilson, *Structure and Immune Recognition of the HIV Glycan Shield.* Annu Rev Biophys, 2018.

22. Wagh, K., et al., *Completeness of HIV-1 Envelope Glycan Shield at Transmission Determines Neutralization Breadth.* Cell Rep, 2018. **25**(4): p. 893-908 e7.
23. Doores, K.J., *The HIV glycan shield as a target for broadly neutralizing antibodies.* The FEBS journal, 2015. **282**(24): p. 4679-4691.
24. Walsh, G., *Biopharmaceutical benchmarks 2010.* Nat Biotechnol, 2010. **28**(9): p. 917-24.
25. Imberty, A. and S. Perez, *Structure, conformation, and dynamics of bioactive oligosaccharides: theoretical approaches and experimental validations.* Chem Rev, 2000. **100**(12): p. 4567-88.
26. Chang, V.T., et al., *Glycoprotein structural genomics: solving the glycosylation problem.* Structure, 2007. **15**(3): p. 267-73.
27. Davis, S.J. and M. Crispin, *Solutions to the glycosylation problem for low-and high-throughput structural glycoproteomics*, in *Functional and Structural Proteomics of Glycoproteins*. 2010, Springer. p. 127-158.
28. Slynko, V., et al., *NMR structure determination of a segmentally labeled glycoprotein using in vitro glycosylation.* J Am Chem Soc, 2009. **131**(3): p. 1274-81.
29. Woods, R.J., et al., *The high degree of internal flexibility observed for an oligomannose oligosaccharide does not alter the overall topology of the molecule.* Eur J Biochem, 1998. **258**(2): p. 372-86.
30. Berman, H.M., et al., *The Protein Data Bank.* Nucleic Acids Res, 2000. **28**(1): p. 235-42.
31. Kumar, S. and P. Cieplak, *Role of N-glycosylation in activation of proMMP-9. A molecular dynamics simulations study.* PLoS One, 2018. **13**(1): p. e0191157.
32. Lee, H.S., Y. Qi, and W. Im, *Effects of N-glycosylation on protein conformation and dynamics: Protein Data Bank analysis and molecular dynamics simulation study.* Scientific reports, 2015. **5**: p. 8926.
33. Dong, C., et al., *Long-ranged Protein-glycan Interactions Stabilize von Willebrand Factor A2 Domain from Mechanical Unfolding.* Sci Rep, 2018. **8**(1): p. 16017.
34. Hang, I., et al., *Analysis of site-specific N-glycan remodeling in the endoplasmic reticulum and the Golgi.* Glycobiology, 2015. **25**(12): p. 1335-49.
35. Ferreira, R.C., et al., *Structural Rearrangements Maintain the Glycan Shield of an HIV-1 Envelope Trimer After the Loss of a Glycan.* Sci Rep, 2018. **8**(1): p. 15031.
36. Yang, M., et al., *Conformational Heterogeneity of the HIV Envelope Glycan Shield.* Sci Rep, 2017. **7**(1): p. 4435.
37. Lemmin, T., et al., *Microsecond Dynamics and Network Analysis of the HIV-1 SOSIP Env Trimer Reveal Collective Behavior and Conserved Microdomains of the Glycan Shield.* Structure, 2017. **25**(10): p. 1631-1639 e2.
38. Berndsen, Z., Chakraborty, S., Wang, X., Cottrell, C., Torres, J., Lopez, C., van-Gills, M., Paulson, J., Gnanakaran, S., Ward, A. B., *Visualization of HIV-1 Env Glycan Shield Across Scales* (submitted for peer review), bioRxiv doi: 10.1101/839217.
39. Zhang, M., et al., *Tracking global patterns of N-linked glycosylation site variation in highly variable viral glycoproteins: HIV, SIV, and HCV envelopes and influenza hemagglutinin.* Glycobiology, 2004. **14**(12): p. 1229-46.
40. Lasky, L.A., et al., *Neutralization of the AIDS retrovirus by antibodies to a recombinant envelope glycoprotein.* Science, 1986. **233**(4760): p. 209-12.
41. Walker, L.M., et al., *A limited number of antibody specificities mediate broad and potent serum neutralization in selected HIV-1 infected individuals.* PLoS Pathog, 2010. **6**(8): p. e1001028.

42. Bradley, T., et al., *Structural Constraints of Vaccine-Induced Tier-2 Autologous HIV Neutralizing Antibodies Targeting the Receptor-Binding Site.* Cell Rep, 2016. **14**(1): p. 43-54.
43. Haynes, B.F., et al., *Progress in HIV-1 vaccine development.* J Allergy Clin Immunol, 2014. **134**(1): p. 3-10; quiz 11.
44. Huang, J., et al., *Broad and potent HIV-1 neutralization by a human antibody that binds the gp41-gp120 interface.* Nature, 2014. **515**(7525): p. 138-42.
45. Pancera, M., et al., *Structure and immune recognition of trimeric pre-fusion HIV-1 Env.* Nature, 2014. **514**(7523): p. 455-61.
46. Julien, J.P., et al., *Crystal structure of a soluble cleaved HIV-1 envelope trimer.* Science, 2013. **342**(6165): p. 1477-83.
47. Lyumkis, D., et al., *Cryo-EM structure of a fully glycosylated soluble cleaved HIV-1 envelope trimer.* Science, 2013. **342**(6165): p. 1484-90.
48. Mouquet, H., et al., *Complex-type N-glycan recognition by potent broadly neutralizing HIV antibodies.* Proc Natl Acad Sci U S A, 2012. **109**(47): p. E3268-77.
49. Walker, L.M., et al., *Broad and potent neutralizing antibodies from an African donor reveal a new HIV-1 vaccine target.* Science, 2009. **326**(5950): p. 285-9.
50. Falkowska, E., et al., *Broadly neutralizing HIV antibodies define a glycan-dependent epitope on the prefusion conformation of gp41 on cleaved envelope trimers.* Immunity, 2014. **40**(5): p. 657-68.
51. Crispin, M. and K.J. Doores, *Targeting host-derived glycans on enveloped viruses for antibody-based vaccine design.* Curr Opin Virol, 2015. **11**: p. 63-9.
52. Pritchard, L.K., et al., *Glycan clustering stabilizes the mannose patch of HIV-1 and preserves vulnerability to broadly neutralizing antibodies.* Nat Commun, 2015. **6**: p. 7479.
53. Pritchard, L.K., et al., *Structural Constraints Determine the Glycosylation of HIV-1 Envelope Trimers.* Cell Rep, 2015. **11**(10): p. 1604-13.
54. Gristick, H.B., et al., *Natively glycosylated HIV-1 Env structure reveals new mode for antibody recognition of the CD4-binding site.* Nat Struct Mol Biol, 2016. **23**(10): p. 906-915.
55. Lee, J.H., G. Ozorowski, and A.B. Ward, *Cryo-EM structure of a native, fully glycosylated, cleaved HIV-1 envelope trimer.* Science, 2016. **351**(6277): p. 1043-8.
56. Barnes, C.O., et al., *Structural characterization of a highly-potent V3-glycan broadly neutralizing antibody bound to natively-glycosylated HIV-1 envelope.* Nat Commun, 2018. **9**(1): p. 1251.
57. Liang, Y., et al., *Changes in Structure and Antigenicity of HIV-1 Env Trimers Resulting from Removal of a Conserved CD4 Binding Site-Proximal Glycan.* J Virol, 2016. **90**(20): p. 9224-36.
58. Cao, L., et al., *Global site-specific N-glycosylation analysis of HIV envelope glycoprotein.* Nat Commun, 2017. **8**: p. 14954.
59. Sanders, R.W., et al., *HIV-1 VACCINES. HIV-1 neutralizing antibodies induced by native-like envelope trimers.* Science, 2015. **349**(6244): p. aac4223.
60. Sanders, R.W., et al., *A next-generation cleaved, soluble HIV-1 Env trimer, BG505 SOSIP.664 gp140, expresses multiple epitopes for broadly neutralizing but not non-neutralizing antibodies.* PLoS Pathog, 2013. **9**(9): p. e1003618.

61. Go, E.P., et al., *Glycosylation Benchmark Profile for HIV-1 Envelope Glycoprotein Production Based on Eleven Env Trimers.* J Virol, 2017. **91**(9).
62. Guvench, O., et al., *CHARMM additive all-atom force field for carbohydrate derivatives and its utility in polysaccharide and carbohydrate–protein modeling.* Journal of chemical theory and computation, 2011. **7**(10): p. 3162-3180.
63. Weinkam, P., J. Pons, and A. Sali, *Structure-based model of allostery predicts coupling between distant sites.* Proc Natl Acad Sci U S A, 2012. **109**(13): p. 4875-80.
64. Guttman, M., et al., *All-atom ensemble modeling to analyze small-angle x-ray scattering of glycosylated proteins.* Structure, 2013. **21**(3): p. 321-31.
65. Eswar, N., et al., *Comparative protein structure modeling using Modeller.* Current protocols in bioinformatics, 2006. **15**(1): p. 5.6. 1-5.6. 30.
66. Sali, A., *Comparative protein modeling by satisfaction of spatial restraints.* Mol Med Today, 1995. **1**(6): p. 270-7.
67. Lütteke, T., M. Frank, and C.-W. von der Lieth, *Carbohydrate Structure Suite (CSS): analysis of carbohydrate 3D structures derived from the PDB.* Nucleic acids research, 2005. **33**(suppl_1): p. D242-D246.
68. Ward, A.B. and I.A. Wilson, *The HIV-1 envelope glycoprotein structure: Nailing down a moving target.* Immunological reviews, 2017. **275**(1): p. 21-32.
69. Bricault, C.A., et al., *HIV-1 Neutralizing Antibody Signatures and Application to Epitope-Targeted Vaccine Design.* Cell Host Microbe, 2019. **25**(1): p. 59-72 e8.
70. Beleva Guthrie, V., et al., *Network analysis of protein adaptation: Modeling the functional impact of multiple mutations.* Molecular biology and evolution, 2018. **35**(6): p. 1507-1519.
71. Huang, L., L. Liao, and C.H. Wu, *Evolutionary analysis and interaction prediction for protein-protein interaction network in geometric space.* PloS one, 2017. **12**(9): p. e0183495.
72. Eargle, J. and Z. Luthey-Schulten, *NetworkView: 3D display and analysis of protein.RNA interaction networks.* Bioinformatics, 2012. **28**(22): p. 3000-1.
73. Skjaerven, L., et al., *Integrating protein structural dynamics and evolutionary analysis with Bio3D.* BMC Bioinformatics, 2014. **15**: p. 399.
74. Sethi, A., et al., *A mechanistic understanding of allosteric immune escape pathways in the HIV-1 envelope glycoprotein.* PLoS Comput Biol, 2013. **9**(5): p. e1003046.
75. Fruchterman, T.M. and E.M. Reingold, *Graph drawing by force-directed placement.* Software: Practice and experience, 1991. **21**(11): p. 1129-1164.
76. Li, Y., et al., *Removal of a single N-linked glycan in human immunodeficiency virus type 1 gp120 results in an enhanced ability to induce neutralizing antibody responses.* J Virol, 2008. **82**(2): p. 638-51.
77. Coss, K.P., et al., *HIV-1 Glycan Density Drives the Persistence of the Mannose Patch within an Infected Individual.* J Virol, 2016. **90**(24): p. 11132-11144.
78. Doores, K.J., et al., *Envelope glycans of immunodeficiency virions are almost entirely oligomannose antigens.* Proc Natl Acad Sci U S A, 2010. **107**(31): p. 13800-5.
79. Warshall, S. *A theorem on boolean matrices*. in *Journal of the ACM*. 1962. Citeseer.
80. Floyd, R.W., *Algorithm 97: shortest path.* Communications of the ACM, 1962. **5**(6): p. 345.
81. Cao, L., et al., *Differential processing of HIV envelope glycans on the virus and soluble recombinant trimer.* Nat Commun, 2018. **9**(1): p. 3693.

82. Schmidt, A.G., et al., *Preconfiguration of the antigen-binding site during affinity maturation of a broadly neutralizing influenza virus antibody.* Proc Natl Acad Sci U S A, 2013. **110**(1): p. 264-9.
83. Xu, K., et al., *Epitope-based vaccine design yields fusion peptide-directed antibodies that neutralize diverse strains of HIV-1.* Nat Med, 2018. **24**(6): p. 857-867.
84. Burton, D.R., et al., *A Blueprint for HIV Vaccine Discovery.* Cell Host Microbe, 2012. **12**(4): p. 396-407.
85. McCoy, L.E., et al., *Holes in the Glycan Shield of the Native HIV Envelope Are a Target of Trimer-Elicited Neutralizing Antibodies.* Cell Rep, 2016. **16**(9): p. 2327-38.
86. Bianchi, M., et al., *Electron-Microscopy-Based Epitope Mapping Defines Specificities of Polyclonal Antibodies Elicited during HIV-1 BG505 Envelope Trimer Immunization.* Immunity, 2018. **49**(2): p. 288-300 e8.
87. Townsley, S., et al., *Conserved Role of an N-Linked Glycan on the Surface Antigen of Human Immunodeficiency Virus Type 1 Modulating Virus Sensitivity to Broadly Neutralizing Antibodies against the Receptor and Coreceptor Binding Sites.* J Virol, 2016. **90**(2): p. 829-41.
88. Huang, X., et al., *Highly conserved HIV-1 gp120 glycans proximal to CD4-binding region affect viral infectivity and neutralizing antibody induction.* Virology, 2012. **423**(1): p. 97-106.
89. Moore, P.L. and C. Williamson, *Approaches to the induction of HIV broadly neutralizing antibodies.* Current Opinion in HIV and AIDS, 2016. **11**(6): p. 569.
90. LaBranche, C.C., et al., *HIV-1 envelope glycan modifications that permit neutralization by germline-reverted VRC01-class broadly neutralizing antibodies.* PLoS Pathog, 2018. **14**(11): p. e1007431.
91. Umotoy, J., et al., *Rapid and Focused Maturation of a VRC01-Class HIV Broadly Neutralizing Antibody Lineage Involves Both Binding and Accommodation of the N276-Glycan.* Immunity, 2019. **51**(1): p. 141-154 e6.
92. Nakagawa, H., et al., *Detection of altered N-glycan profiles in whole serum from rheumatoid arthritis patients.* J Chromatogr B Analyt Technol Biomed Life Sci, 2007. **853**(1-2): p. 133-7.
93. Taniguchi, N. and Y. Kizuka, *Glycans and cancer: role of N-glycans in cancer biomarker, progression and metastasis, and therapeutics.* Adv Cancer Res, 2015. **126**: p. 11-51.
94. Dalziel, M., et al., *Emerging principles for the therapeutic exploitation of glycosylation.* Science, 2014. **343**(6166): p. 1235681.
95. Bhatia, R., et al., *Cancer-associated mucins: role in immune modulation and metastasis.* Cancer Metastasis Rev, 2019. **38**(1-2): p. 223-236.
96. Kwon, Y.D., et al., *Crystal structure, conformational fixation and entry-related interactions of mature ligand-free HIV-1 Env.* Nat Struct Mol Biol, 2015. **22**(7): p. 522-31.
97. Garces, F., et al., *Affinity Maturation of a Potent Family of HIV Antibodies Is Primarily Focused on Accommodating or Avoiding Glycans.* Immunity, 2015. **43**(6): p. 1053-63.
98. Laskowski, R.A., et al., *PROCHECK: a program to check the stereochemical quality of protein structures.* Journal of applied crystallography, 1993. **26**(2): p. 283-291.

99. Best, R.B., et al., *Optimization of the additive CHARMM all-atom protein force field targeting improved sampling of the backbone ϕ, ψ and side-chain $\chi1$ and $\chi2$ dihedral angles.* Journal of chemical theory and computation, 2012. **8**(9): p. 3257-3273.
100. Huang, J. and A.D. MacKerell Jr, *CHARMM36 all-atom additive protein force field: Validation based on comparison to NMR data.* Journal of computational chemistry, 2013. **34**(25): p. 2135-2145.
101. Rossum, G., *Python reference manual.* 1995.
102. MATLAB, *MATLAB, Version R2018a*. 2018, The MathWorks Inc Natick, MA.
103. Pillai, S.U., T. Suel, and S. Cha, *The Perron-Frobenius theorem: some of its applications.* IEEE Signal Processing Magazine, 2005. **22**(2): p. 62-75.
104. Newman, M.E., *Modularity and community structure in networks.* Proceedings of the national academy of sciences, 2006. **103**(23): p. 8577-8582.
105. Newman, M.E. and M. Girvan, *Finding and evaluating community structure in networks.* Physical review E, 2004. **69**(2): p. 026113.
106. Blondel, V.D., et al., *Fast unfolding of communities in large networks.* Journal of statistical mechanics: theory and experiment, 2008. **2008**(10): p. P10008.

Figures and Figure Legends

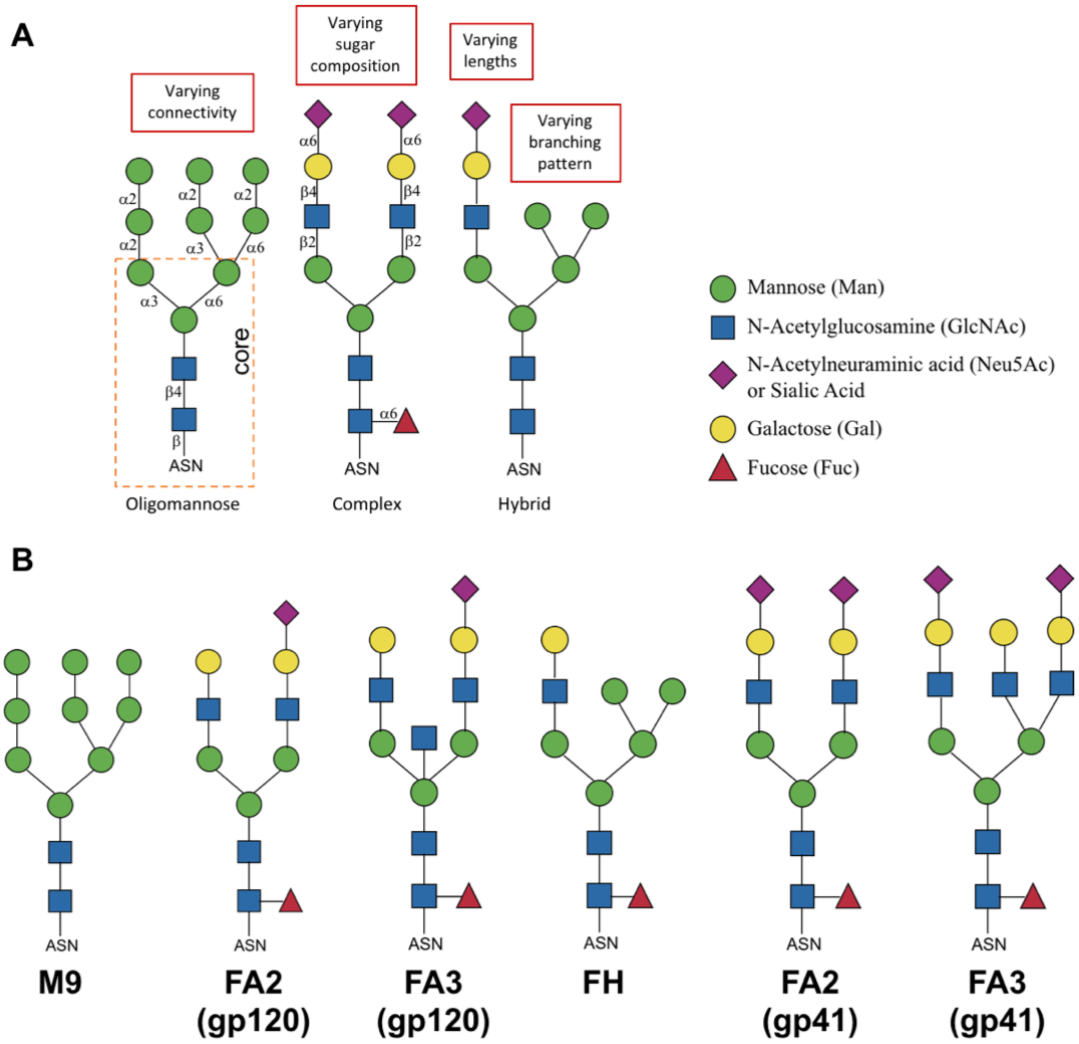

Figure1: Schematic representation of N-glycan types. (a). The three generalized N-glycan types commonly found in glycoproteins are high oligomannose, complex, and hybrid (having a mix of oligomannose and complex branches). The common core of Man3GlcNAc2Asn is indicated. Variability of these glycans stem from varying connectivity, sugar composition, lengths and branching patterns. (b). The glycan species selected for different sites of the BG505 native model (as given in Table S1). M9 ≡ mannose-9, FA2 ≡ fucosylated two-antennae, FA3 ≡ fucosylated three-antennae, FH ≡ fucosylated hybrid. It must be noted that the complex glycans in gp41 (N611, N618, N625, N637) are different from those in gp120, as per site-specific mass spectroscopy experiments.

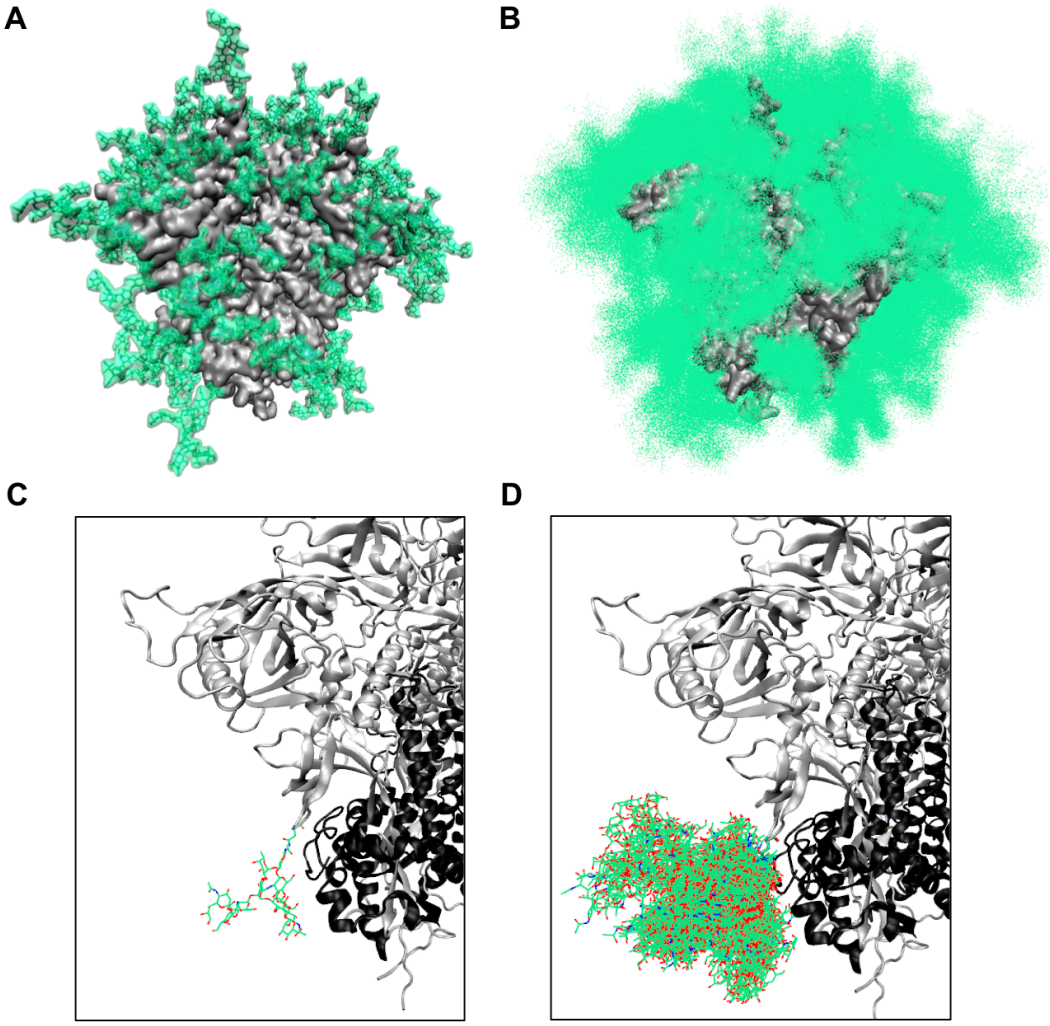

940

941

942 **Figure 2: Spatial shielding of Env protein by glycans.** (a) A single snapshot of modeled natively
943 glycosylated BG505 structure, with each glycan taking up a particular conformation. Protein
944 surface in grey, glycans in green. (b) Cumulative shielding effect over time due to the flexible and
945 dynamic nature of the glycans. 100 randomly selected models from the 1000-structure ensemble
946 is shown here. (c) Glycan N88 in one particular pose. gp120 (grey), gp41 (black), glycan carbon
947 atoms (green), glycan oxygen atoms (red), glycan nitrogen atoms (blue). (d) Spatial sampling by
948 glycan N88. Each glycan can take a variety of different conformations and orientations, sampling
949 a large volume in space.

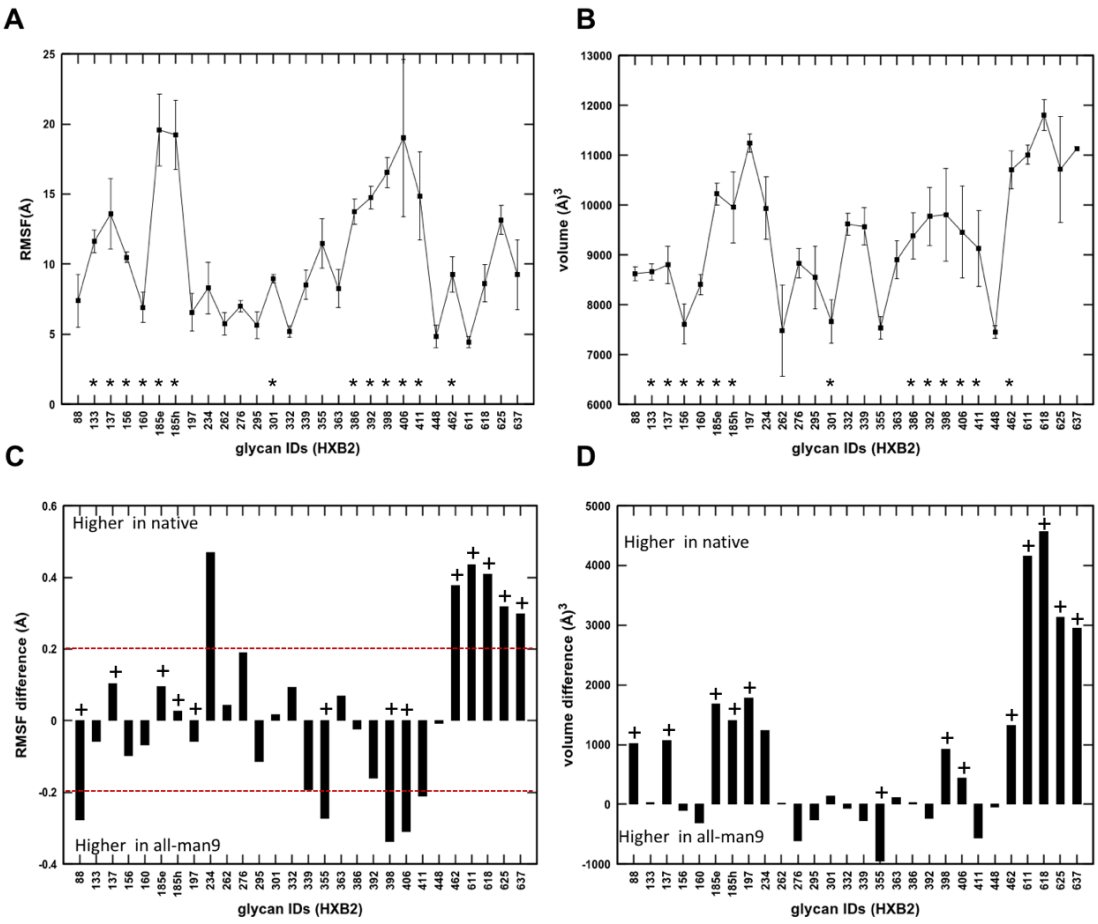

Figure 3: Structural fluctuations of individual glycans in BG505 native model. Glycans present in the hyper-variable loop regions of gp120 are indicated by *. Glycans modeled as fucosylated complex or hybrid glycoforms are indicated by +. (a) Site-specific Root Mean Squared fluctuations (RMSF). (b) Sampled volume per glycan at each PNGS. (c) Difference in RMSF between native and all-man9 model. Native minus all-man9 values are plotted. (d) Difference in sampled volume between native and all-man9 model. Native minus all-man9 values are plotted.

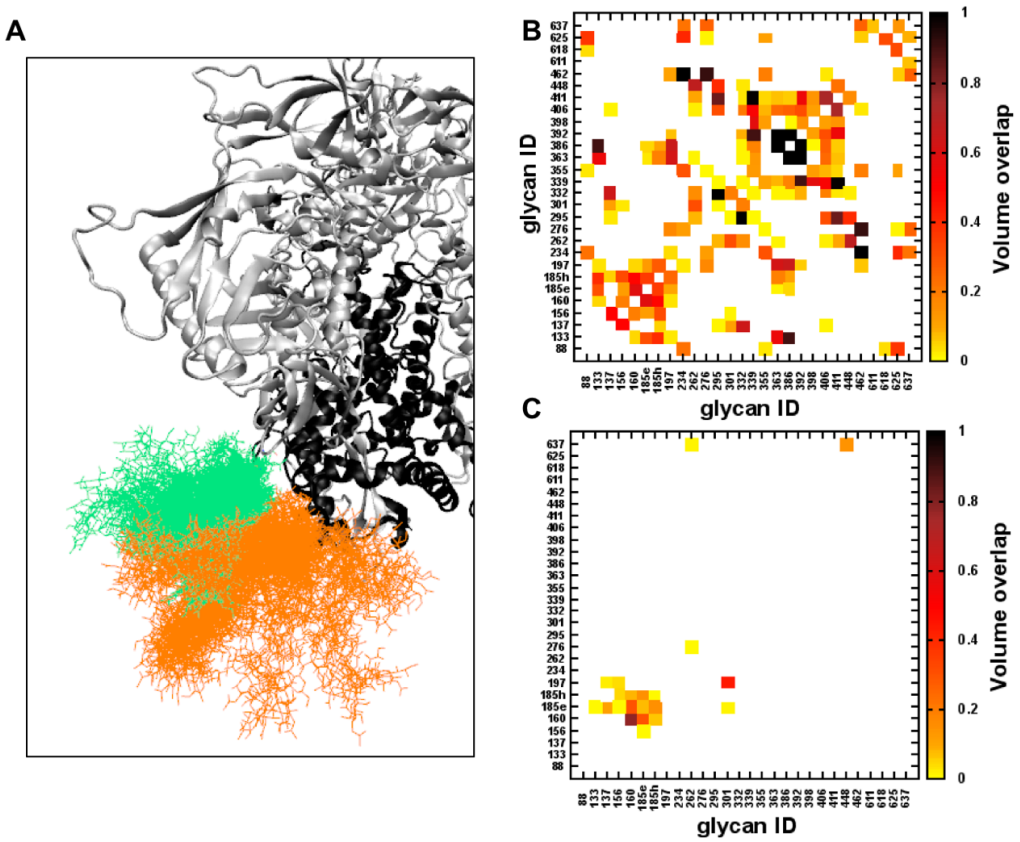

958

959

960 **Figure 4: Glycan-glycan volume overlap.** (a) Neighboring glycans within close proximity can
961 sample overlapping volumes. Glycan N88 shown in green and glycan N625 shown in orange.
962 gp120 (grey) and gp41 (black) are shown in cartoon representation. (b) Probability distribution
963 map of inter-glycan fractional overlap within a single protomer, and (c) between inter-protomer
964 glycans.

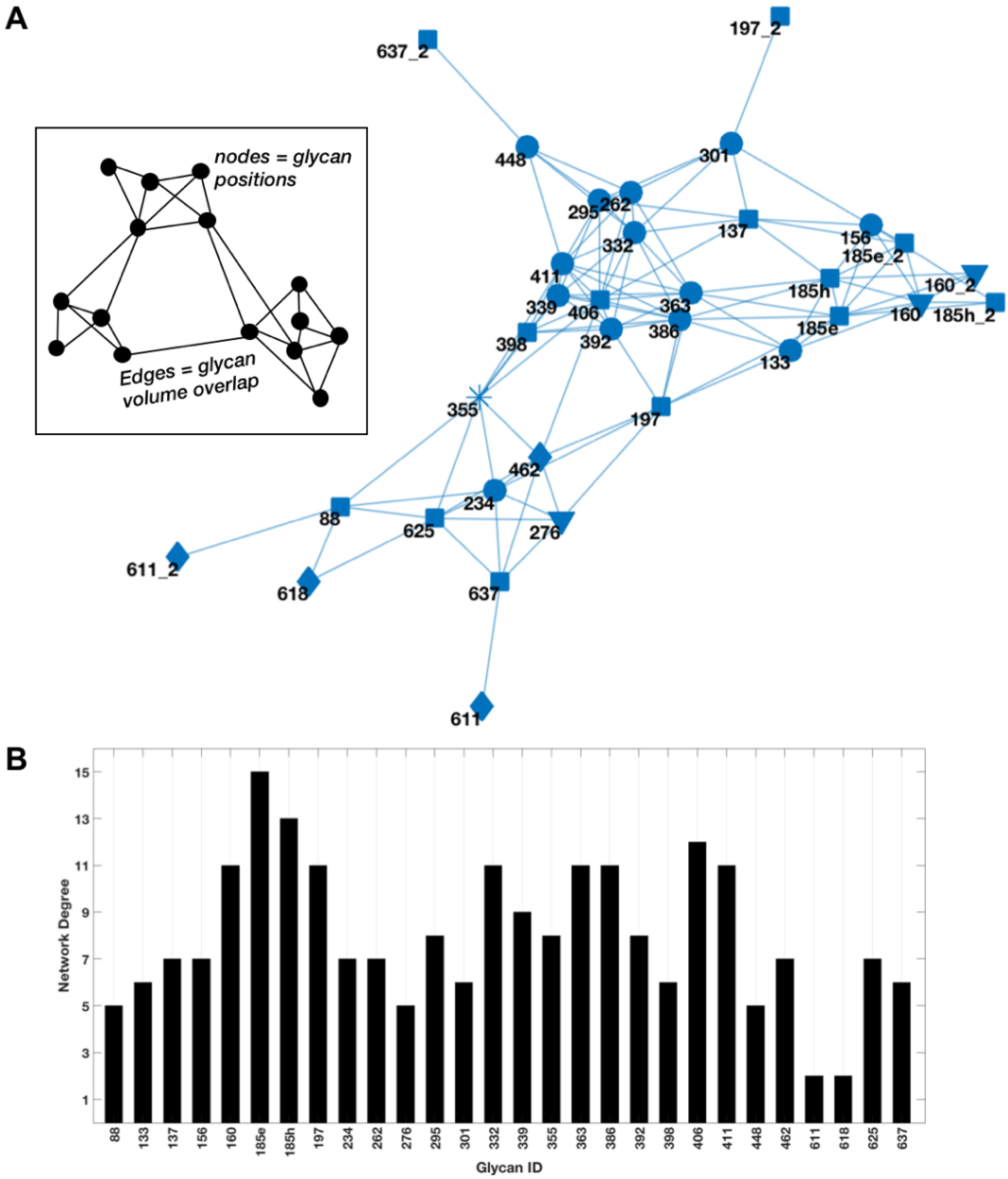

965

966

967 **Figure 5: Spatial network of BG505 native glycosylation.** (a) Visual representation of network
968 in 2-dimensions, based on a force-directed layout. Each glycan forms a node-point on the graph,
969 two nodes are connected by an edge (inset, from reference [38], Fig.8) if there is interaction as per
970 Figure 4B and C, scaled by the fraction of overlap. (b) The network degree of each node or glycan,
971 given by the number of other nodes it is connected to.

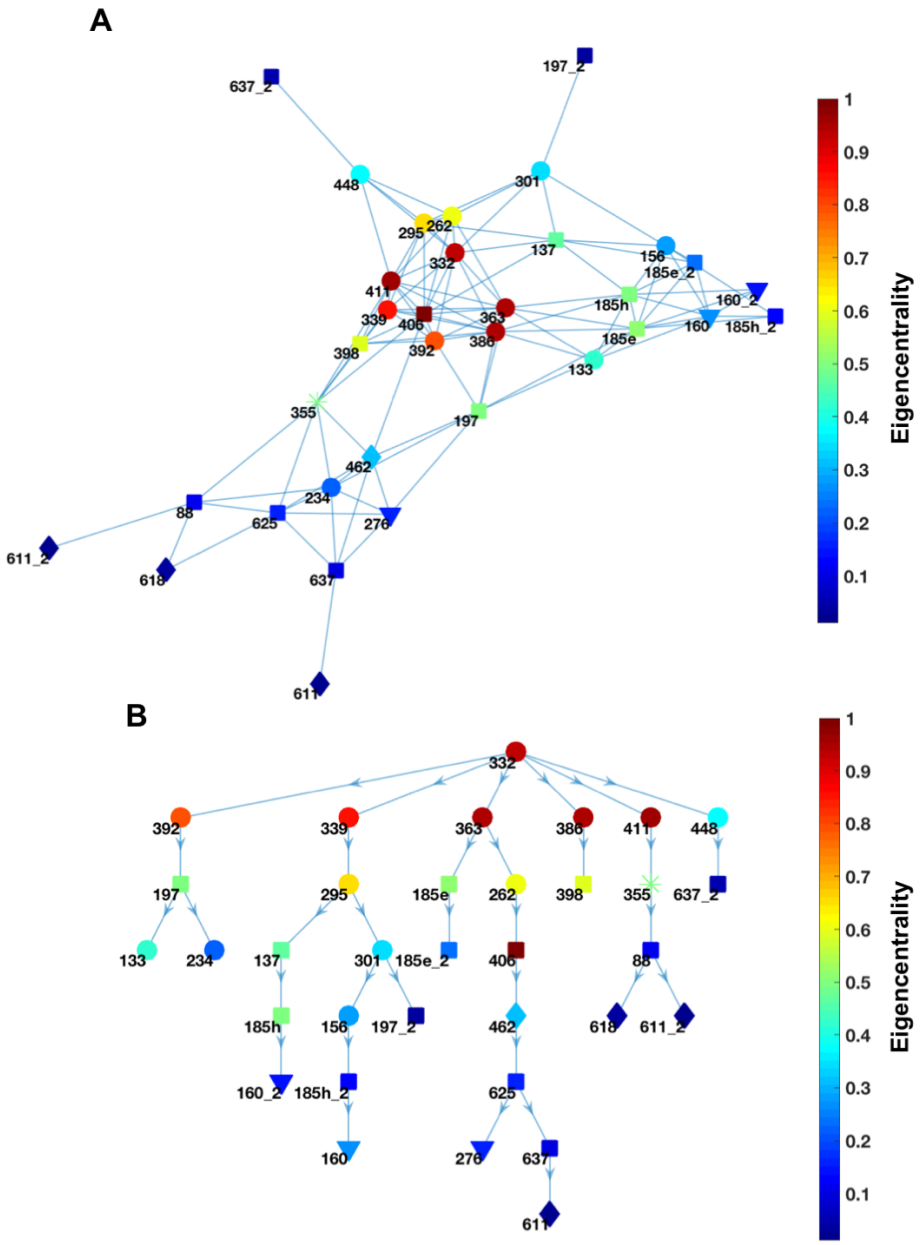

Figure 6: BG505 native glycan network properties. (a) Normalized eigenvector centrality of the glycans projected on the network. (b) Shortest path of communication between glycan N332 and all other glycans in the network.

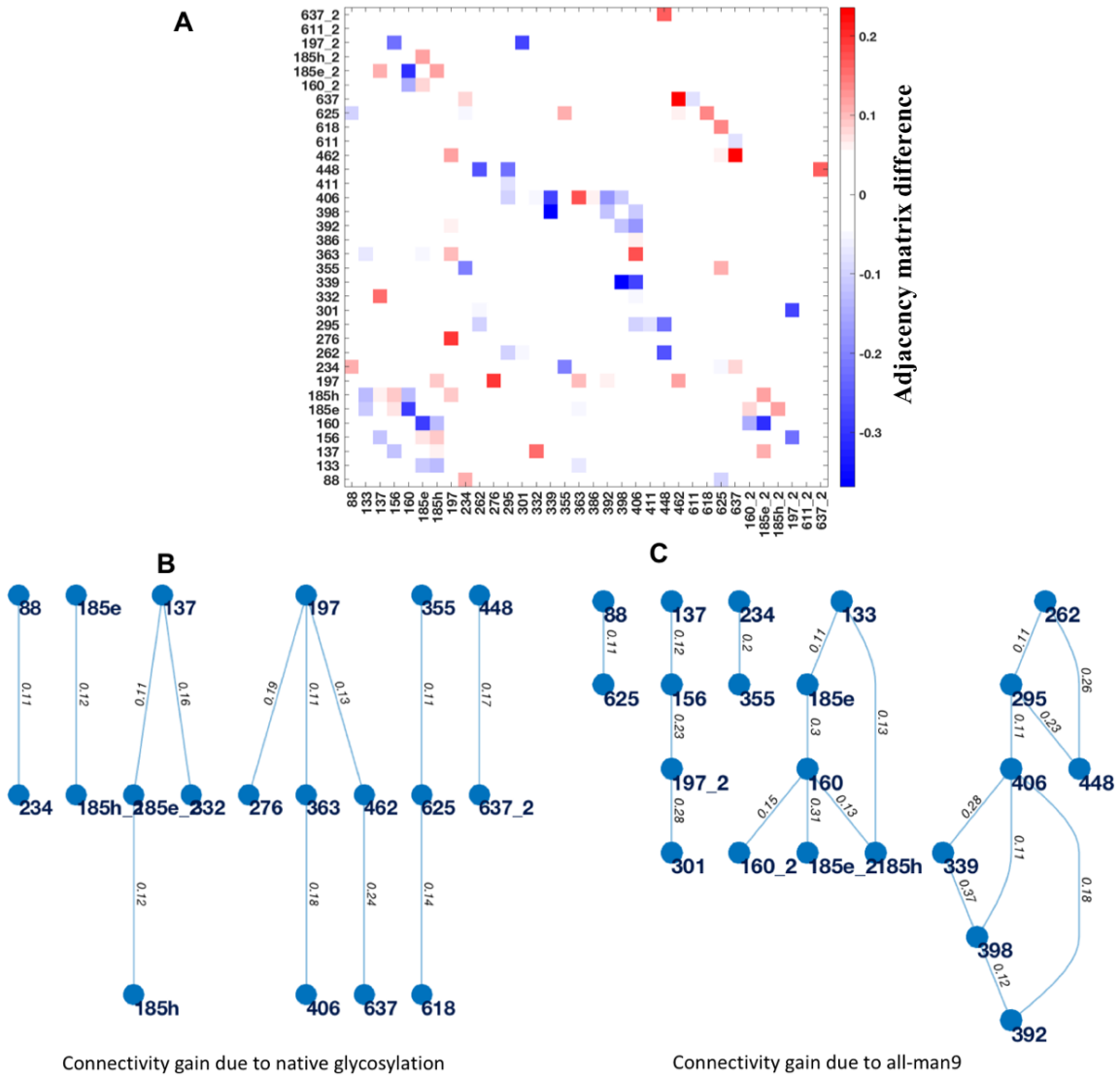

Figure 7: Network difference between native and all-man9 glycosylation. (a) Difference in adjacency matrices between the two models, - native minus man9. Blue color indicates at least 5% decrease in edge weight, and red indicates at least 5% increase in edge weight in native network, as compared to all-man9. (b) Increase and (c) decrease in connectivity due to native glycosylation in comparison with all-man9 model.

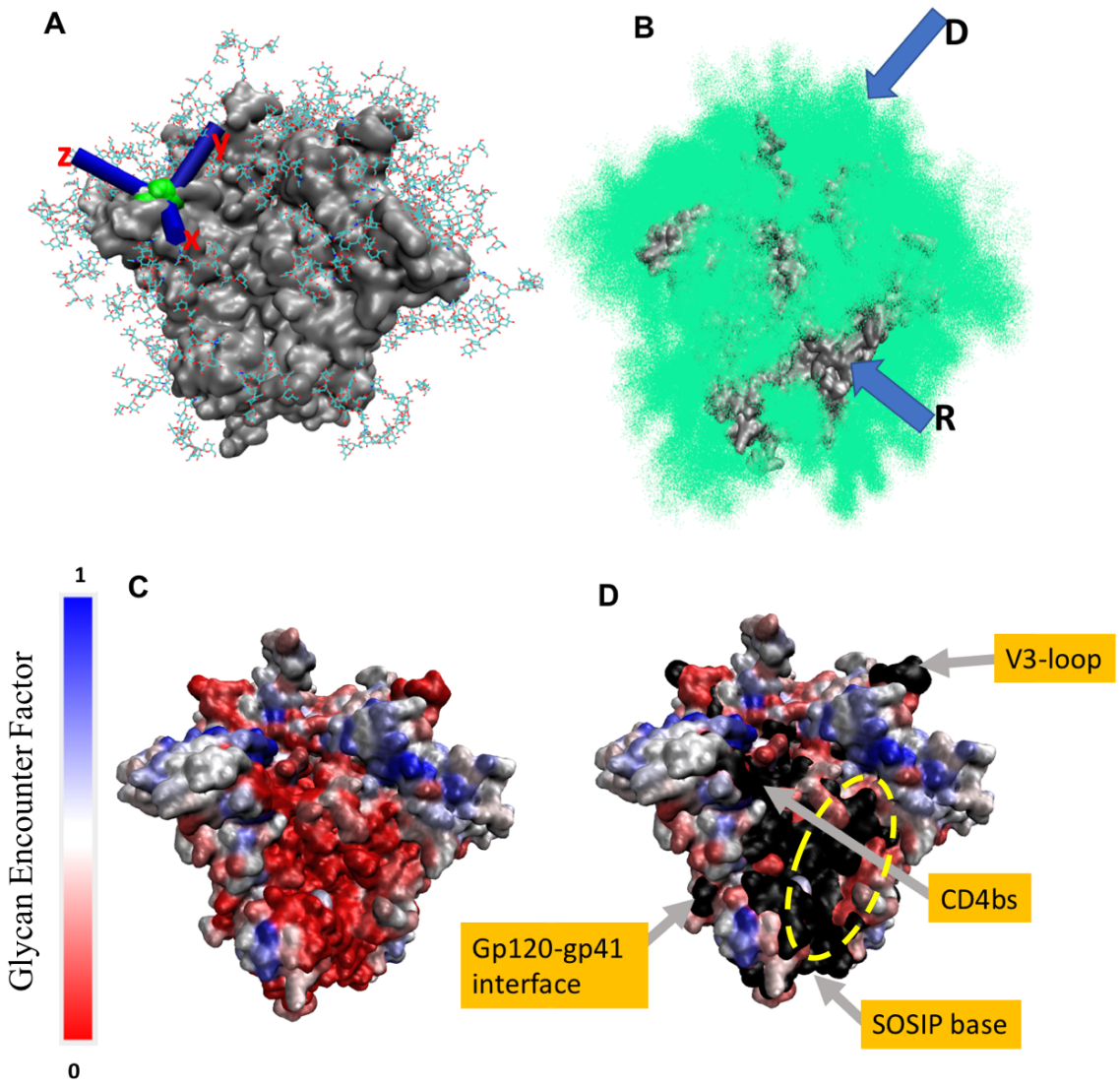

Figure 8: Glycan Encounter Factor (GEF) for quantifying shielding effect. (a) At each residue present on the surface of the protein, the approaching probe is considered in three directions **x, y** and **z.** (b) Any point on the surface which has a dense glycan covering, such as D, has a high glycan encounter factor value, versus a point such as R where the glycan covering is sparse, which will have a low GEF. (c) Representation of normalized GEF on Env surface, given by a colormap. (d) Regions of BG505 surface having a GEF less than 1.5 (normalized GEF <0.14) is colored in black. Typical known antibody epitopes are indicated by arrows. BG505-specific GH and COT epitope region demarcated by yellow dashed circle.

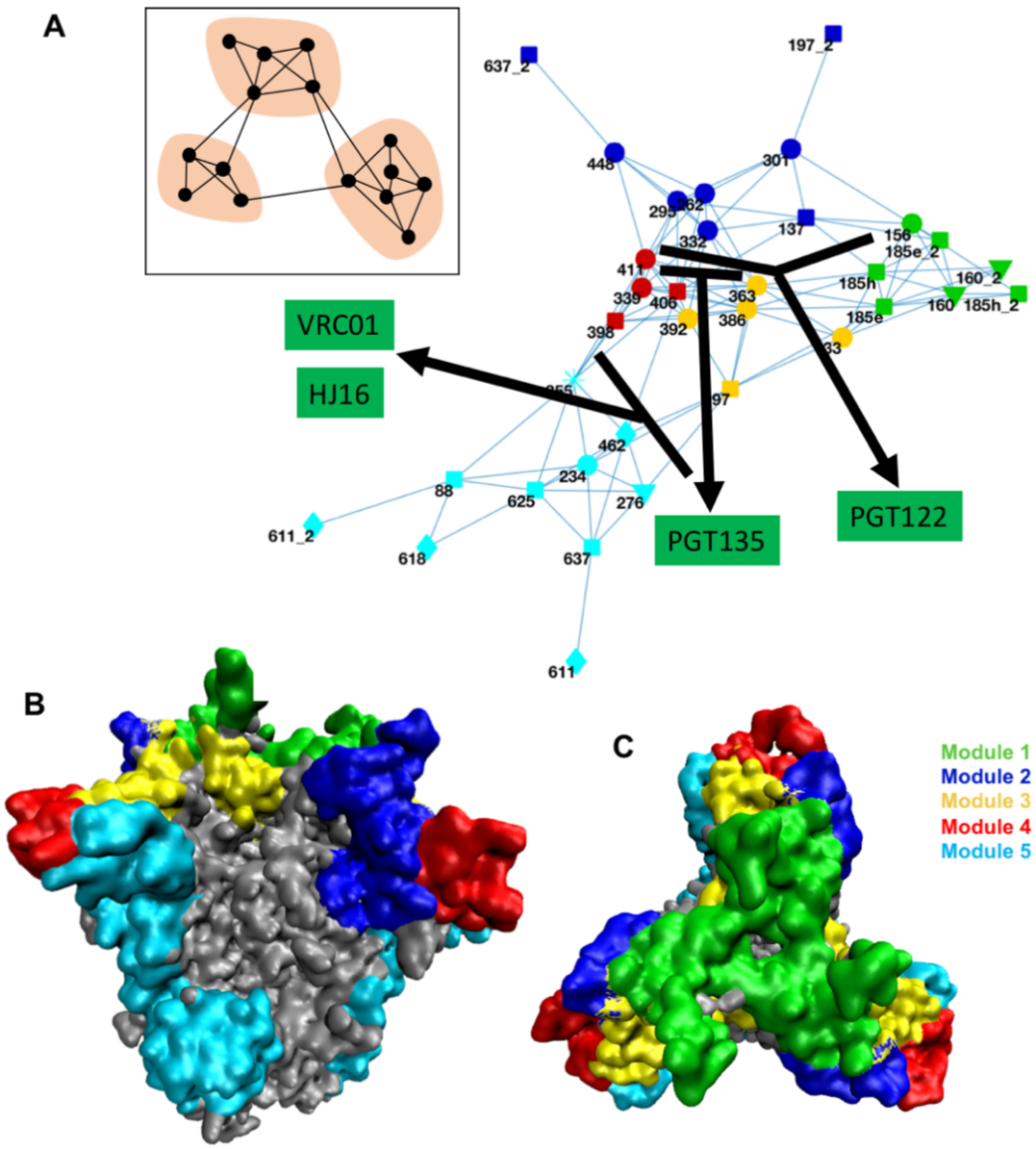

992

993

994 **Figure 9: Subcommunities within network.** (a) 5 different subcommunities were identified
995 based on modularity maximization. The sub-community junctions identify susceptible regions in
996 the shield where antibodies tend to bind. (b) Location of each sub-community projected on the
997 Env surface, including the (c) top view.

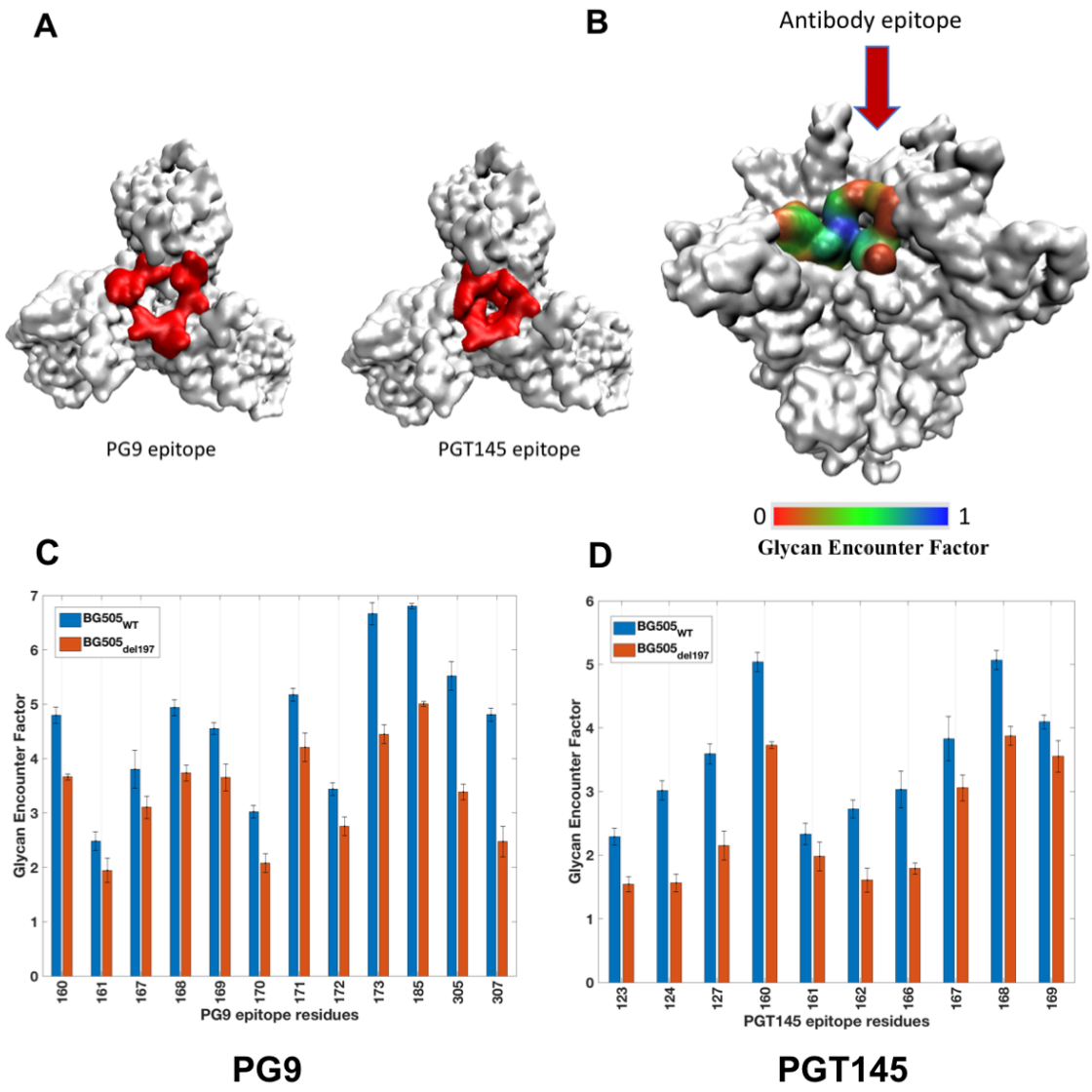

998

999 **Figure 10: Deletion of glycan N197 decreases glycan shielding at PG9 and PGT145 epitope.**
1000 (a) Top view of Env showing epitope regions of antibodies PG9 and PGT145 at the apex. (b)
1001 Footprint of glycan N197 on Env surface, colored by glycan encounter factor contributed by N197
1002 alone. (c) Normalized glycan encounter factor over the PG9 and (d) PGT145 epitope residues.
1003 GEF decreases for both the epitopes due to deletion of N197 glycan.